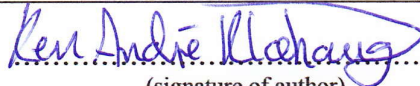# Universitetet i Stavanger

FACULTY OF SCIENCE AND TECHNOLOGY

MASTER'S THESIS

Study programme/specialisation: Automation and Signal Processing	Spring semester, 2018 Open
Author: Ken André Klæhaug	*(signature of author)*
Programme coordinator: Karl Skretting Supervisor(s): Karl Skretting, Dan Sui	
Title of master's thesis: Data and control tuning of a laboratory-scale autonomous drilling rig Norwegian title: Data- og kontroll- innstilling av autonom laboratorieskala borerigg	
Credits: 30	
Keywords: Vibration, Torsional drill string model, Kalman filter, electromagnetic interference, electromagnetic compatibility, Drillbotics, drilling rig	Number of pages: ....67............ + supplemental material/other: ...11... Stavanger, 15. June 2018 date/year

Data and control tuning of a laboratory-scale autonomous drilling rig

Data- og kontroll- innstilling av autonom laboratorieskala borerigg

Ken André Klæhaug

June 14, 2018

Abstract

The main focus of this thesis is to tune a lab scale autonomous drilling rig. The rig requires a robust control architecture that can manage unforeseen risks and problems, and at the same time optimize the systems performance to maintain a high rate of penetration (ROP). Such the small scale drilling rig requires very short reaction time, for fault detection and problem management to achieve good performances. This thesis goes in to the dynamic process modelling, electromagnetic interference shielding and data filtering required to run the real-time lab scale autonomous drilling rig.

Results show that the simulations made in this thesis of the torsional vibration drill string is close to real torque measurements. Kalman filter has also been implemented, and show that it can give better WOB accuracy while drilling. Electromagnetic compatibility (EMC) has been improved and results in better data quality, giving more accurate controller parameters, which have increased the ROP on the small scale drilling rig.

Ken André Klæhaug

Stavanger, June 14, 2018

Acknowledgments

Contents

Abbreviations

AC/DC Alternating Current/Direct Current

BHA Bottom Hole Assembly

CAN Controller Area Network

CCS Conined Compressive Strength

DAC Digital to Analog Conversion

DAQ Data Acquisition

DOF Degrees of Freedom

DSATS Drilling Systems Automation Technical Section

EMC Electromagnetic compatibility

EMI Electromagnetic interference

HMI Human Machine Interface

I/O Input/Output

LC Load Cell

MISO Multiple Input Single Output

MOSI Multiple Output Single Input

MSE Mechanical Specific Energy

PCB Printed circuit Board

PID Proportional, Integral, Derivative

PLC Programmable Logical Controller

ROP Rate of Penetration

RPM Revolutions Per Minute

SCK Serial Clock

SPE Society of Petroleum Engineers

SPI Serial Peripheral Interface

SS Slave Select

TD Top Drive

UCS Uniaxial Compressive Strength

UIS University of Stavanger

USB Universal Serial Bus

WOB Weight on Bit

List of Figures

List of Tables

Chapter 1

Introduction

Since the beginning of the oil and gas adventure, it have had an enormous impact in the daily life of people all around the globe. Since then, technologies also evolved exponentially. Today we have technologies to develop advanced systems, replacing people from dangerous site work, thus making a safer environment offshore. The new technology will also ideally increase performance of an oil rig and also reduce production and high downtime expenses.

Available technology includes advanced control systems, and intelligent algorithms. This technology has the potential to monitor multiple processes and execute commands with better performance and precision than a human. Therefore development of new machines also requires significant amount of testing now as before. Especially since it has the goal of replacing humans in production, and operate autonomously. Autonomous drilling has come interesting for the oil and gas industry, since cost of production has increased and oil prices decreased for the last couple of years.

1.1 Background

Drilling Systems Automation Technical Section (DSATS) of SPE has made an competition; named Drillbotics for inrernational universities to contribute with their ideas and design of an autonomous drilling rig. For this competition, University of Stavanger (UiS) has made a laboratory-scale drilling rig, which made it to the finals in 2017, and received a strong 3rd place.

Improving the drilling rig is therefore the main focus for team UiS in the 2018 Drillbotics competition. In order to improve the performance, electrical-/control- system and mechanical designs must be robust. Understanding how the rig operates and knowing the limitations, in addition to theoretical conditions, are the key for better performance. Changes to the overall rig design is also carried out for the competition; old ideas and new changes to the rig are further carried out in Chapter 2 - Rig Design.

This thesis will focus on the mathematical dynamic model of the drill string, to further understand and control the rig performance.

1.1.1 Problem formulation

Listed is the problems to be studied and improved for this thesis:

- Mathematical model of the drill string,

- Electromagnetic interference,

- Filtering, Kalman filter,

- Control system.

It is observed that sensor measurements sometimes are out of synchronization during real time operations. Some measurements arrive early or late due to sensor malfunctions etc. Due to these inconsistent sampling frequencies of different measurements, the weight on bit (WOB) will fail to maintain correct regulations. Improvements can be made to maintain correct WOB, and are listed:

- Reduce electromagnetic interferance. Cables and junction box have to be moved away from the source and shielded. The effects of EMI can cause increase in error rate to a total loss of the data. Since the source is very close to the sensors and micro-controllers, EMI must be reduced.

- Kalman filter can be implemented to further improve the data quality and control parameters.

- An optimal control algorithm can be integrated to sufficiently regulate theoperational parameters of the system. Parameters regulate the performance which the rig is able to drill through different rock formations. To optimize the system, two PID-controllers are considered; Revolutions per minute (RPM) control and WOB control.

- Study and make a mathematical model of the process; drill string, in order to estimate parameters and mitigate vibrations. This is under a theoretical assumption, without being dependant on the drilling rig, according to challenges listed in section 1.1.2 and 1.2.

1.1.2 Previous challenges

Key challenges in transforming the system from semi-autonomous to fully autonomous:

- Bad data quality.

- Insufficient data, especially for near-bit torque, bit vibrations and pipe deformation.

- Finding relevant mathematical models for the scale of the system .

- Designing, tuning and implementing PID controller to control WOB.

- Detecting a formation change through drilling.

- Detection and especially mitigation of extensive vibrations, buckling etc.

1.2   Key challenges

Key challenges are the new implementations that are carried out by the group or individual thesis work, to improve the rig for the 2018 competition. These challenges also make the rig inoperative for a longer time period. They include:

- Main upgrade of the rig is re-location of fuse box, which was originally placed beside a motor on the rig top plate.

- Included in the re-location, is to replace all wires going to the fuse box with shielded wires, as well as "cleaning" wires inside the fuse box.

- Mechanical upgrades; drill string, circulation system, etc.

- Re-write all code to Python from C-sharp (C#).

- Experiments and testings regarding Phd. and thesis studies.

1.3   My contributions

My contribution to the project has been, giving a mathematical model of the drill string. It also goes into the measures of shielding the rig in order to reduce EMI as well as the use of Kalman filter to improve sensor data. Besides the thesis work, collaboration in getting the rig fully functional for the competition. Listed is the main focus of the thesis:

- Making a mathematical model and a new control system design in Chapter 4, Control and modelling.

- Experimenting and compare results with the real data in Chapter 5, Experiments and results.

- Re-wireing and shield the rig, as well as being available for other implementations to the rig.

1.4 Organization of the thesis

Thesis is organized as follows:

- Chapter 2; Rig design, explains the different parts and functions of the drilling rig.

- Chapter 3; Theory of subject that needs more details.

- Chapter 4; Control and modelling, is the main focus of the thesis, describing control system and mathematical model of torsional drill string dynamics.

- Chapter 5; Experiments and results of theories and simulation model.

- Chapter 6; Conclusion.

Chapter 2

Rig Design

This chapter gives a overview and specifications of different parts on the rig, and equipment installed. Parts of the rig that are specifically of interest for this thesis is the rotation system, vibrations, DAQ amplifier and EMI. Other parts of this section are common work of the project group. A through and detailed thesis of the rig design, was done by group members, see te details in their bachelor's thesis. [7]
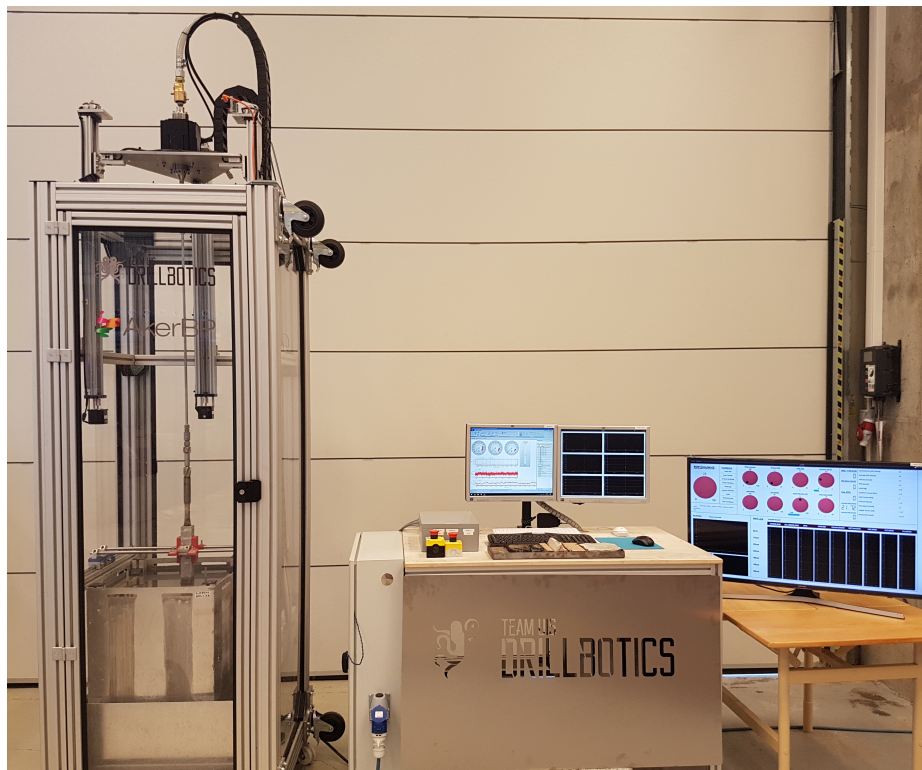
Figure 2.1: Picture of the autonomous lab-scale drilling rig 2018.

Figure 2.1 shows the 2018 team UiS drilling rig. A good rig design is very important whether it involves full scale drilling rigs or laboratory small scale rigs. Laboratory rigs, if design properly,

can simulate a full scale rig adequate, but many problems regarding full scale rigs can also be neglected. That involves for example high temperatures in the wellbore, gravity regarding WOB or high pressures. Even on the laboratory rig, some problems are very important to handle, and the most crucial for operation is vibrations. Vibrations from the drill pipe is also a crucial part of problem handling on full scale rigs, since big vibrations can destroy the wellbore or equipment; vibrations have the potential of destroying the whole rig, if not correctly handled.

Overall design of the rig, see fig. 2.2, is made to test a small scale rig relatively good, autonomously. On the laboratory rig it is possible to test theories and problems regarding drilling in a safe environment, and compete in the yearly Drillbotics competition.
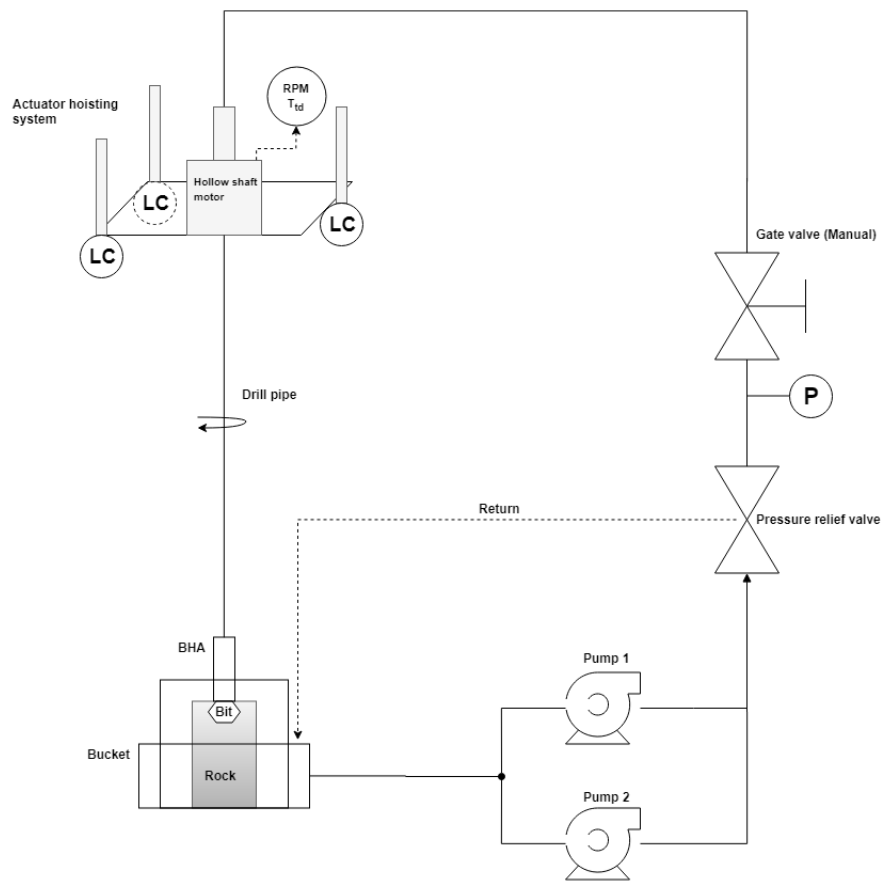
Figure 2.2: Rig Design schematic. **LC** - Load cell sensor, **P** - Pressure transmitter, T_{td} - Top drive torque.

2.1 Drilling

2.1.1 Rotation

Mathematical modelling of the torsional drill string dynamics is calculated and deduced in section 4.2.1. The whole drill string is limited to; *Round Aluminum Tube 3/8 inch diameter x 36 inches long; 0.049 inch wall or equivalent,* in accordance to restrictions in the competition rules. [8]
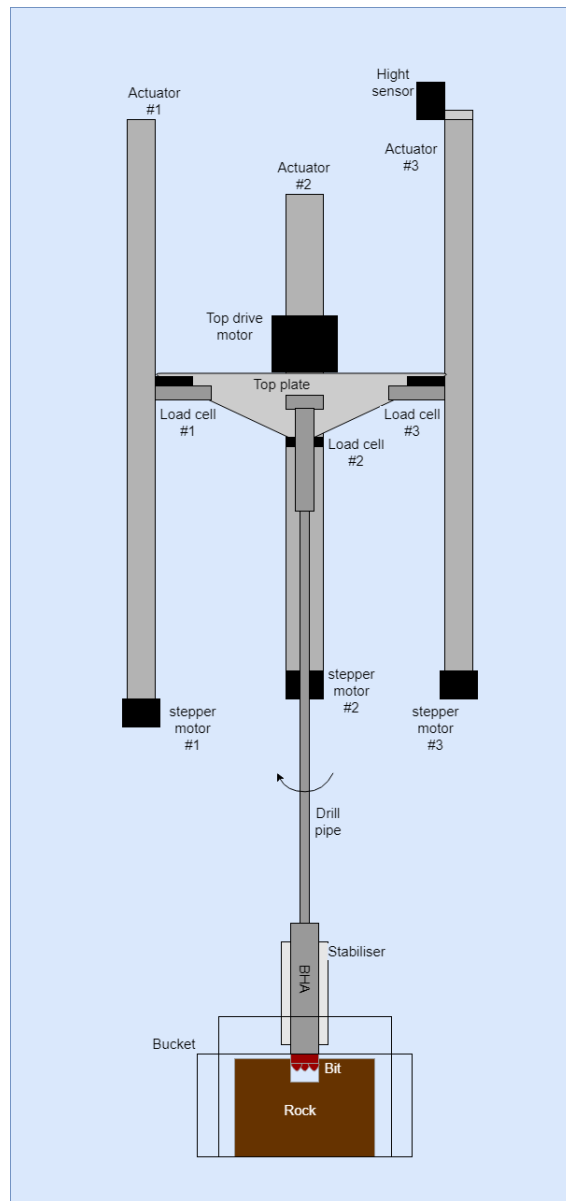
Figure 2.3: Rotational system schematic.

In figure 2.3 motor on the top plate rotates the drill pipe, and is restricted to limitations through

a motor driver. Reason for the limitation is that the pipe may twist-off during long drilling sessions. As the speed increases, the risk of twist-off also increases if the drill bit suddenly gets stuck. Drill bit is designed in the matter to reduce vibrations and increase the ROP.

2.1.2   Top Drive

Figure 2.4: Top drive of the laboratory rig.

A top drive (TD), see fig. 2.4, is an hollow-shaft drilling machine, making it possible to circulate drilling fluids in the borehole while drilling. On the laboratory rig, a hollow-shaft brushless motor, **APM-HE09ACH**, is classified as the TD. To prevent decrease in ROP, and potential twist-off, torque and RPM are limited in a driver. The driver calculates the dynamic motor model and sends torque/RPM feedback to a PLC (Arduino DUE).

To control the top drive motor a driver **XDL-L7PA008UE** is installed. The driver makes it possible to control top drive motor accurately, being able to set limitations to torque and RPM.

Figure 2.5: Top drive driver, XDL-L7PA008UE from LS industrial systems.

The driver takes care of the mathematical modelling of the motor, giving the correct measurements for torque and RPM, and easy control of the motor. This relieves the PLC of heavy calculations, which would cause delays. Measurements for RPM and torque are further received by the HBM-DAQ amplifier and are used for monitoring and calculations; UCS, MSE, etc.

2.2 Hoisting system
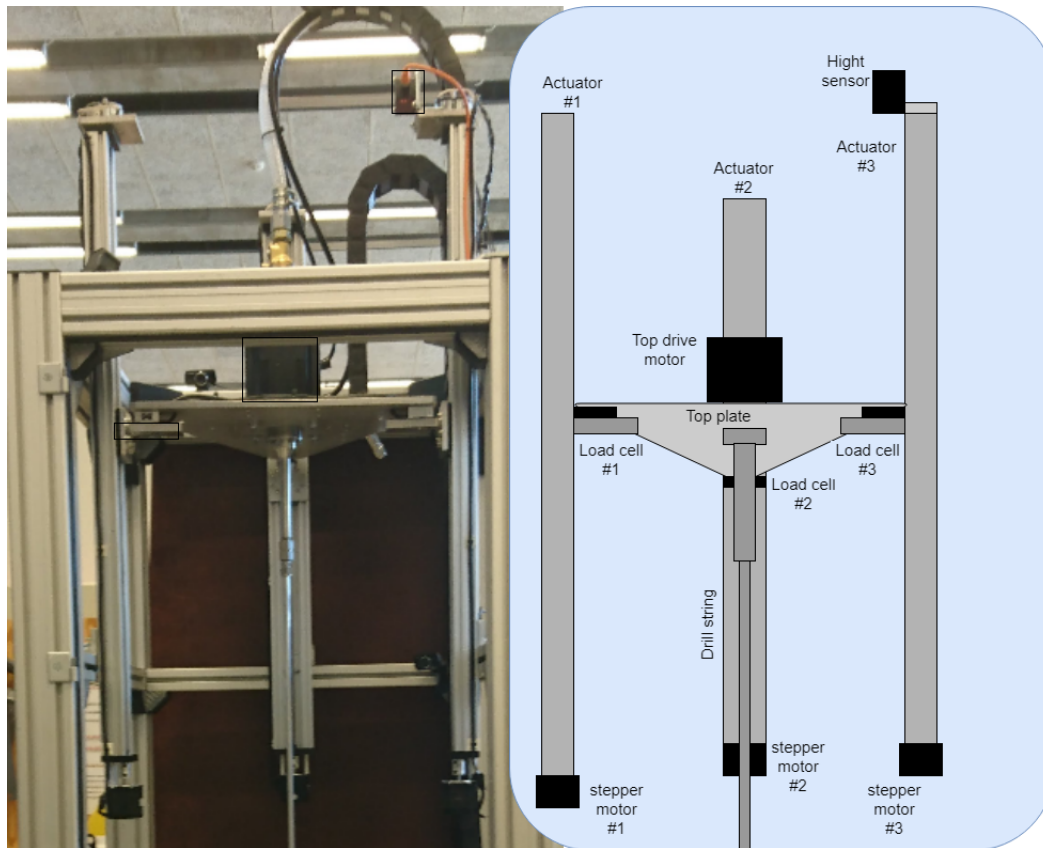
Figure 2.6: Hoisting of the top deck, with load cells on each actuator.

Hoisting system is to move the drill string and to maintain force on the bit to penetrate the formation, or relieve force on the bit. As Figure 2.6 shows, a top deck is placed between three actuators, which is controlled by three synchronized *Nema 23* stepper motors; one for each actuator. As for other equipment placed on the top deck, there is the top drive and three load cells. The load cells are located under the top deck, which measure force on bit and total weight of top deck and equipment mounted under it. Each motor further communicates with an Arduino micro-controller which receives set-point parameters from calculations depending on WOB, ROP and MSE.

2.3 Circulation system

Liquid is pumped from the tank with two synchronous pumps to prevent overheating, a bigger pump was proposed, but the price and the size of the pump was to extensive. Further the liquid flows through a pressure relief valve, which bleeds off liquid to the tank if the pressure gets to high. In Figure 2.7 sensor "P" measures the pressure of the system, which is used to

control the pumps. The manual gate valve is used to simulate overpressure, in which the pressure sensor measures the pressure build-up. The liquid then flows through an hollow-shaft motor, through the drill string, where the liquid increases the dampening factor and stiffens the pipe. At last the liquid ends up down-hole, to remove cuttings and lubricate the hole.

The circulation can contain oil and/or other substances, to help for better performance of the rig. The substance in the circulation system also lubricate the hole and prevent the bit/BHA to exceed high temperature. Due to safety and spill possibility, the circulation contains water through testing and experiments in this year competition.
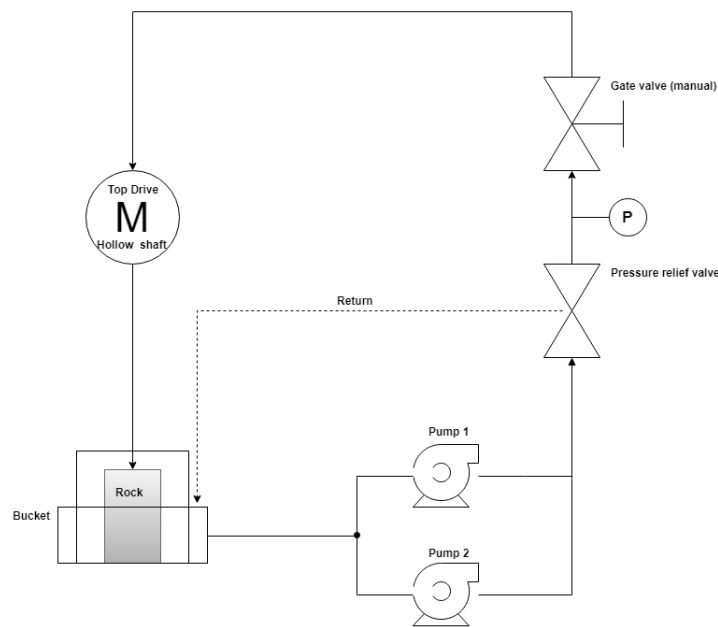
Figure 2.7: Complete circulation schematic.

The old design had problems with the pump overheating when drilling, which shutdown the pump for few seconds. By shutting down circulation, problems will occur in the hole, which also adds downtime in the overall operation. The new design now contains two identical pumps to prevent overheating, and will only be operated one at a time.

2.4   Control system equipment

2.4.1   Arduino DUE
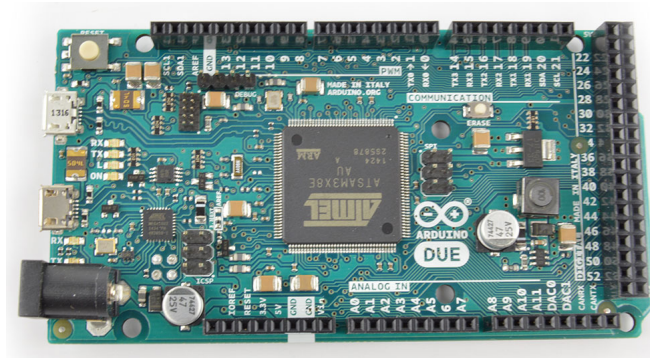
Description	Limit range
Micro-controller	AT91SAM3X8E
Operating Voltage	3.3V
Input Voltage (recommended)	7-12V
Input Voltage (limits)	6-16V
Digital I/O Pins	54 (12 PWM output)
Analog Input Pins	12
Analog Output Pins	2 (DAC)
Total DC Output Current on all I/O lines	130 mA
DC Current for 3.3V Pin	800 mA
DC Current for 5V Pin	800 mA
Flash Memory	512 KB
SRAM	96 KB (two banks: 64KB and 32KB)
Clock Speed	84 MHz
Length	101.52 mm
Width	53.3 mm
Weight	36 g

Figure 2.8 & Table 2.1: Arduino DUE specifications [1]

Arduino DUE is a 32-bit ARM micro-controller, made as an open source environment for commercial use and research purposes. The micro-controller has 54 input/output pins, where 12 can be used as PWM outputs. In addition to the I/O pins, the board also has 2 pins for digital-to-analog conversion capability (DAC). Connection to the board is done via the micro-USB port to an external computer. There are three options of powering the micro-controller; safest alternatives are with an power jack or micro-USB cable. The most risky powering method is with a battery or AC/DC-adapter, since too high current may fry the

micro-controller. Arduino DUE can also be used to power sensors either by outputting 0-3.3V signal or 5V, directly from the pins. [1]

Arduino is known for their big network of programmers, using the micro-controller in both simple and advanced systems. Because of the popularity, libraries have been developed, to make it even better to use, as well as guides on "how to...". Arduino DUE micro-controller is also popular because of performance reliability, with the capability to execute heavy calculations in complex systems. Since the micro-controller delivers a flash memory of 512 KB and an 84 MHz clock, the micro-controller may have difficulties doing time-critical operations, and at the same time doing heavy calculations.

2.4.2   HBM QuantumX

Figure 2.9: 8-channel HBM QuantumX MX840B

HBM QuantumX MX840B is an 8-channel DAQ amplifier with individual channel configuration. The channels can be used to measure sensor data from a wide range of sensors; pressure, rotational speed, thermal, etc. QuantumX uses a "Plug & Measure" technology, to automatically identify any connections, and immediately start measuring. Some of the main features is a sampling rate of 40 kS/s and signal bandwidth of 7 kHz, making it suitable for analyzing and measuring of electrical and mechanical vibrations; in addition to noises in the time, frequency and angle domain.[9]

2.4.3   Sensors

Other sensors not listed in this section is the torque and RPM, which are mentioned in section 2.1.2.

Load Cells

Load cells are used to measure WOB and to detect and measure vibrations while drilling. Implemented on the rig is three **FNZ 0-100N (X/Y/Z-100N)** LC, each with force sensors; F_x, F_y and F_z direction.
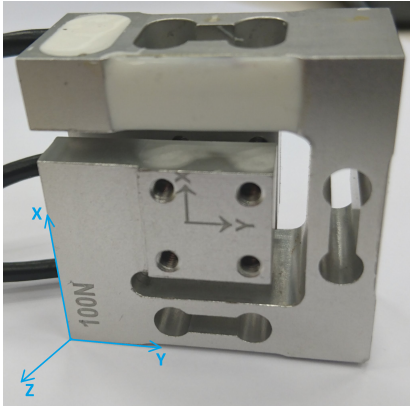
Description	Limit range
Sensor	FNZ 0-100N (X/Y/Z-100N)
Capacity	100N
Rated output (approx.)	1.0 mV/V
Non-linearity	±0.05%
Hysteresis	0.1%
Non-repeatability	±0.05%
Ingress protection	IP62

Figure 2.10 & Table 2.2: triaxial load cell specifications. [2]

The load cells are implemented under the top plate on each actuator, making the capacity up to $300N$ for tension and compression.

Height

The height sensor, *SICK Distance Sensor Dx35*, is placed at the top of the rig pointing downwards to the top plate. The height sensor calculates the distance the top plate travel, thus giving an indication of the depth drilled. This only gives a rough approximation of the depth til the down-hole tool is in operation.

Table 2.3: Height sensor specifications.

Description	Limit range
Measuring range	50 - 1200 mm (90% remission)
Resolution/-analog output	0.1 mm/12 Bit
Accuracy	±10 mm
Output rate	1 - 32 ms
Response time	2.5 - 96.5 ms
Switching frequency	333 - 6 Hz
Power consumption	$\leqslant 1.7\ W$
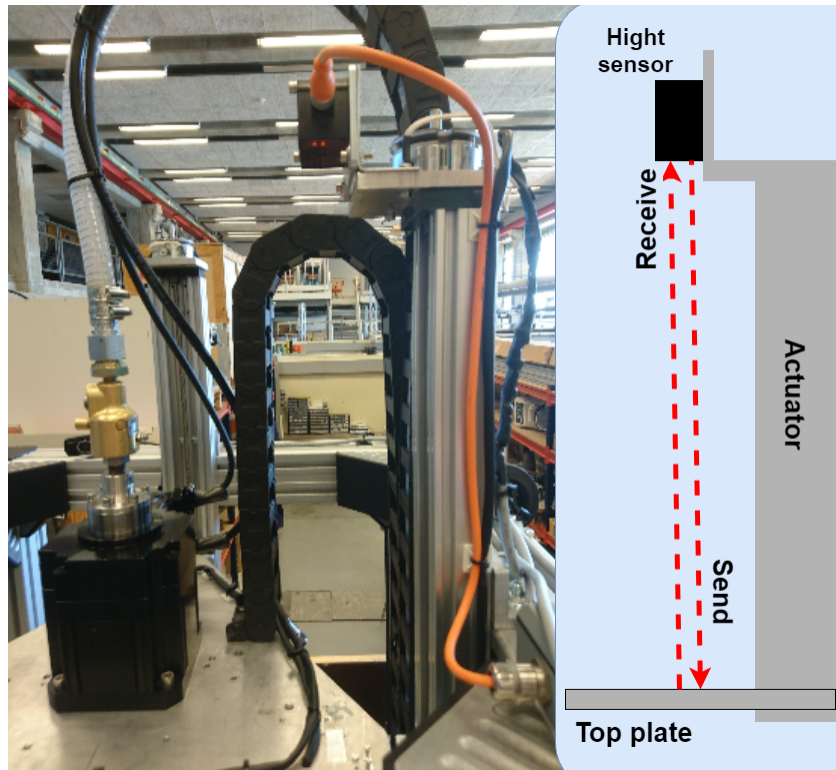
Figure 2.11: Hoisting of the top deck, with load cells on each actuator.

Pressure

A pressure transmitter, **Gems Series 3100**, is used in order to detect leak or an over pressure scenario. The pumps in the circulation system have a cut-off pressure of 3.1 *bar*, but the built in pressure transmitter in the pumps can not detect a leak scenario. Pressure transmitter also ensures that the circulation system operates within the desired threshold. Since the pumps provide maximum flow rate as default, the transmitter must calculate the flow rate as a function of pressure. This lowers the flow rate by opening the leak-off valve gradually to achieve the desired pressure.
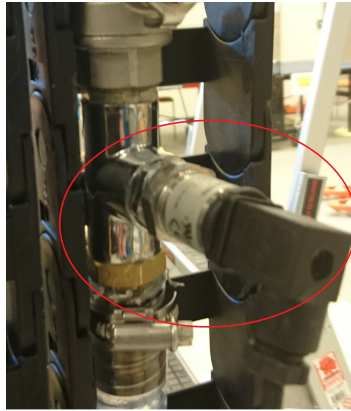
Figure 2.12: Pressure transmitter; Gems Series 3100.

Down-hole measurement

Down-hole tool is a new implementation and is designed by Simen Jøsang Nilsen and Ole André Hjelm in their master's thesis.

Figure 2.13: Down-hole tool, BHA with printed circuit board (PCB) housing, containing accelerometer and micro-controller.

Down-hole tool contain PCB with a micro-controller and accelerometer, the PCB is designed so that it can fit inside the BHA close to the bit. This makes it possible to receive real-time data from the well. The accelerometer is used to detect uncertainties in the formation, bit speed and vibrations, and send the data to a micro-controller on the PCB with SPI protocol. Micro-controller then converts the data and sends it to the surface with CAN2.0B protocol, where the data is logged into a database. [10]

2.5 Drilling problem management

Delays in operation is highly crucial, therefore fault detection and management is very important. In an autonomous environment, the machine must carry out work, that is usually done semi-automatically on full scale rigs in operation. The most common problems that the control system has to detect and manage are happening in the well. Since the focus is the laboratory small scale drilling rig, only problems relevant to this rig are discussed. General problems on full scale rigs are more complex and may be irrelevant in laboratory; such as temperature, which is negligible. In addition to drilling critical problems, EMI is also a serious problem on the laboratory scale drilling rig. EMI effects the data received, making the drilling operation imprecise. The disturbance is further explained in section 3.3 and how it can be dealt with.

2.5.1 Vibrations

Calculating and measuring vibrations on the drill-string can be very complex, and is therefor an entire subject in drilling theory. To handle the vibrations, one can model the different types of vibrations, to further control/reduce the actions causing vibrations. There are three types of vibrations; axial, torsional and lateral.
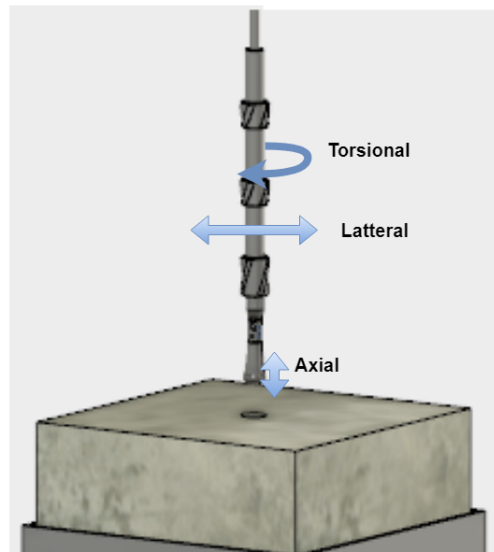
Figure 2.14: Drilling schematic.

Axial vibrations is caused when the bit bounces up and down, thus creating shockwaves along the drill-string. This type of vibration can cause damage to the bit and BHA, and may also lead to reduced ROP. The material of the drill-string reduces (dampens) the vibrations. It is recommended to reduce RPM and increase WOB, in order to maintain high ROP. [11]

Lateral vibrations are caused by whirl, when the drill-string moves in the transverse direction. The lateral vibrations can cause damage to the bit, BHA and wellbore, when the drill-string rotates off the borehole geometric center. Whirl can be differentiated into; bit whirl, BHA whirl, forward and backward whirl. Bit whirl is the result of bit crating greater hole than the bit diameter, thus making the bit move freely in the hole. If the BHA is smaller than the wellbore it can create BHA whirl, which may result in forward or backward whirl if the drill-string bends. Forward whirl is vibrations in the same direction as the drill-string rotates, backward whirl is seen in the opposite direction. To reduce the lateral vibrations, a stiffer BHA can prevent motion in the transverse direction. To prevent damage it is recommended to stop drilling til the vibrations fade away. In general, one can also reduce RPM and increase WOB if lateral vibrations occur. [11]

Torsional vibrations are caused by frictional torque on bit and BHA in relative to the rock formation, which is also known as stick slip. This type of torque decelerates the bit and drill-string, but are re-accelerated, which can cause the bit to have a much higher RPM than the TD. Stick slip can be described as an jerking motion, when two surfaces are sliding over each other; for instance screeching brakes on a car. This problem is rarely seen in vertical wells, and can cause severe damage to the bit and drill-string, which also causes the ROP to decrease rapidly. In order to maintain drilling, reduce WOB and increase RPM. [11]

2.5.2 Twist-off

A twist-off occurs if the drill bit gets stuck; comes to a forced stop, or stick slip, which makes TD torque exceed limitations of the drill-string (over-torque).

2.5.3 Pack-off

Occurs if the wellbore around the drill string gets clogged, caused by wellbore collapsing around drill-string or inadequate transportation of cuttings.

2.5.4 Key seating

Is a typical problem when drilling deviation wells, because the drill collars, stabilizers or drill string wears into the wellbore. It is a combination of rotating the drill string and side forces imposed to the wellbore.

2.5.5 Overpull

Caused by the bit or stabilizers being stuck in the wellbore. This may damage the drill-string by stretching it vertically, and may also do harm to actuators.

2.5.6 New formation

Different rock formations may cause damage to the bit or drill string, previous mentioned problems may occur if not handled correctly. A new formation is detected by the system with a sudden increase or decrease in ROP. This leads to change in the calculation of uniaxial compressive strength (UCS) when a formation is detected. Founder points is found by sweeping RPM and WOB to reach the optimal ROP.

2.5.7 Bit balling

Typically caused by to high WOB and shale formations (clay) in addition to poor bit-design. Because of inadequate transportation of cuttings, the drill bit becomes covered in cuttings. Reduces ROP since the drill bit grind the surface of the formation rather than cut into it. If bit balling occurs; pick off bottom, lett the bit hydraulics to clean the cutters, continue drilling with higher RPM and lower WOB. [11]

2.6 Rate of penetration

When drilling a full scale well on-/off-shore; or small scale wells in laboratory, with advanced drilling machines, it is important to always maintain a safe operation while drilling. To maintain a safe operation, restriction to ROP is calculated. ROP measures how quick the drill bit can deepen the wellbore, without risking life, environment and equipment. In practice and on the laboratory small scale rig, it is important to maintain a high ROP as possible, when accounting for cost and efficiency.[12] . ROP is defined as change in bit depth, $dh(t)$, versus change in time, dt, given in feet per hour or meters per hour.

Equation for the instantaneous ROP is defined:

$$ROP(t) = \frac{dh(t)}{dt} \tag{2.1}$$

2.7 Formation detection

Uses calculations of MSE and UCS to detemine a new formation

Mechanical specific energy

MSE is a measurement which determine the amount of energy required to drill a certain volume of rock. [13]

Todd Robert Hamrick have deduced the equation transformation in his report [13] from 2011 on page 10. As proposed, MSE is derived as energy input divided by volume removed:

$$MSE = \frac{Energy \quad input}{Volume \quad output}$$ (2.2)

On the lab scale drilling rig, UCS and CCS is equal to one another, caused by lack of pressure on the rock sample. MSE is calculated from ROP, WOB, torque on bit and rotational speed. [14]

Uniaxial Compressive Strength

UCS is used to evaluate a material's maximum axial compressive stress, before failing. The measure gives an estimate of the material strength [15]. Figure 2.15 is a table describing the rock classification, given a UCS measurement. [3]

Grade	Description	UCS	$I_{s(50)}$	Field identification	Rock types
R6	Extremely strong rock	>250	> 10	Specimen can only be pull apart by a geological hammer	fresh basalt, chert, diabase, gneiss, granite, and quartzite
R5	Very strong rock	100 - 200	4 - 10	Specimen requires many blows of geological hammer to fracture it.	amphibiolite, sandstone, basalt, gabbro, gneiss, granodiorite, limestone, marble, rhyolite, and tuff
R4	Strong rock	50 - 100	2 - 4	Specimen requires more than one blow by geological hammer to fracture it.	limestone, marble, sandstone, and schist
R3	Medium strong rock	25 - 50	1 - 2	Cannot be scraped or peeled with a pocket knife; specimen can be fractured with a single firm blow of a geological hammer.	phyllite, schist, siltstone
R2	Weak rock	5 - 25	-	Can be peeled by a pocket knife with difficulty; shallow indentations made by firm blow with a point of geological hammer.	chalk, rock salt, claystone, marl, siltstone, schist
R1	Weak rok	1 - 5	-	Crumbles under firm blows with point of geological hammer; can be peeled by pocket knife	highly weathered or altered rock, schist
R0	Extremely weak rock	0,25 - 1	-	Indented by thumbnail.	stiff fault gouge

UCS – uniaxial compressive strength [MPa]; $I_{s(50)}$ – strength index [MPa]

Figure 2.15: Determination of UCS by hand held accessories.[3]

On the lab scale drilling rig, a down-hole tool have been implemented, to be able to detect new rock formation in real-time. To calculate the UCS on the rig, a surveillance system is in place, to calculate the approximate UCS [MPa] for formations. Calculation of UCS is based on the bit-torque and ROP, and uses a approximate friction factor ranging between 0.84 and 0.93 [14].

2.8   Human machine interface

To operate the drilling rig, all commands and alerts are handled through the HMI. The interface is divided into seven sections, seen in figure 2.16.
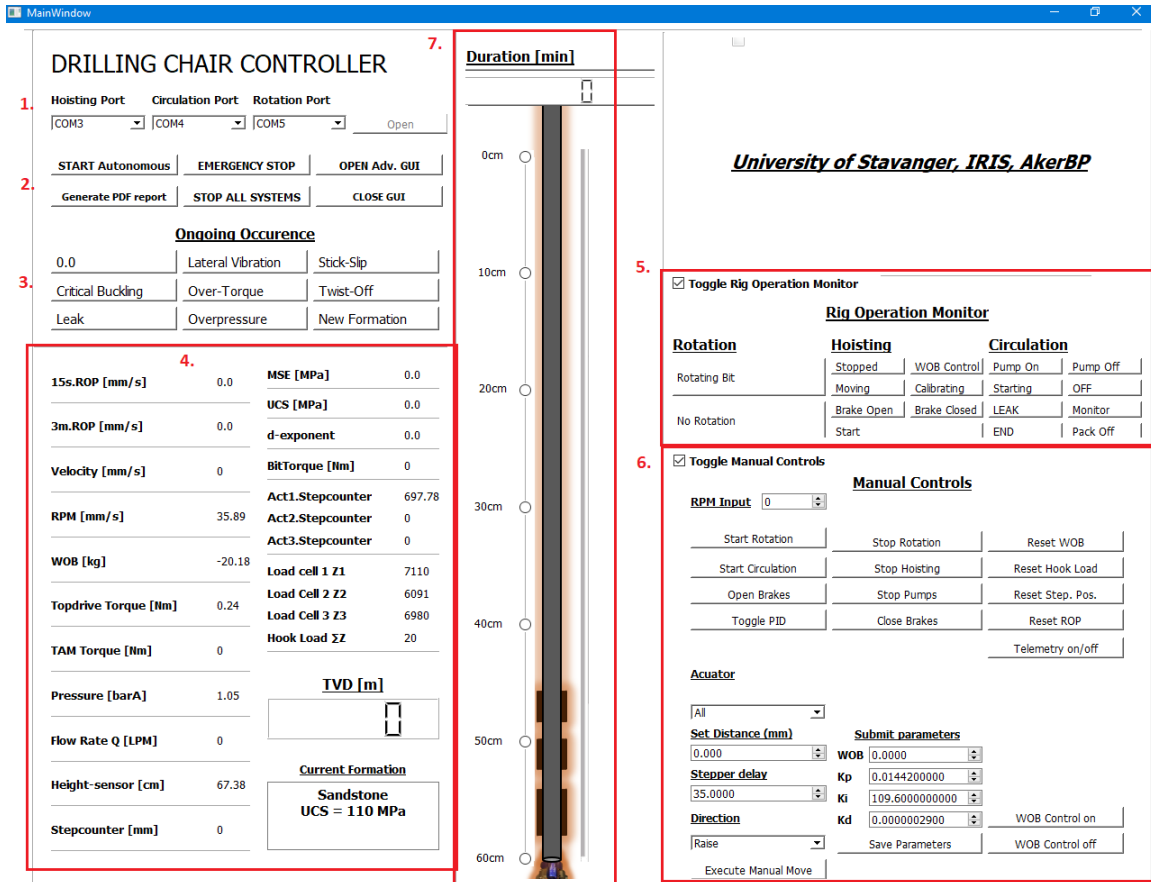
Figure 2.16: HMI design, control panel.

1. **Communication ports**

   COM. port drop-down tabs lets the user choose which input port (USB port) on the computer a micro-controller uses.

2. **Start autonomous mode/Emergency stop**

   START Autonomous tells the drilling rig to operate autonomously, and is mainly used for the competition. *Generate PDF report* makes a well log and of the current operation. *Emergency Stop* is a precaution in addition to a physical emergency stop switch, which will stop the whole operation if a dangerous situation occurs. *STOP ALL SYSTEMS*, same as emergency stop but do not shut the power off.

3. **Ongoing occurrence**

   Highlight a condition, this is to tell the control system to handle accordingly, in addition to give a warning of potential drilling problems.

4. **Monitoring data, real-time values**

   Data is also stored in a database for further being analyzed, the numbers gives the current value of a sensor/measurement. At this point the *Current formation* section is not used.

5. **Rig operation monitor**
   Highlight the current state of the operation.

6. **Manual controls**
   This panel is not operational in autonomous mode. Manual controls is mainly used to test the drilling rig in faults, critical conditions and testing.

7. **Operation time and distance drilled**
   Gives an indication of the total drilling operation and the distance the rig has drilled into a formation. Note: longest distance is set to 60 *cm*, which is the depth of the competition sample formation.

Visualization of the operation state is shown in figure 2.17. This screen shows analog-/digital-measurements, and real time plots. Plots are placed horizontally in order to have an easy visualization of the current depth.
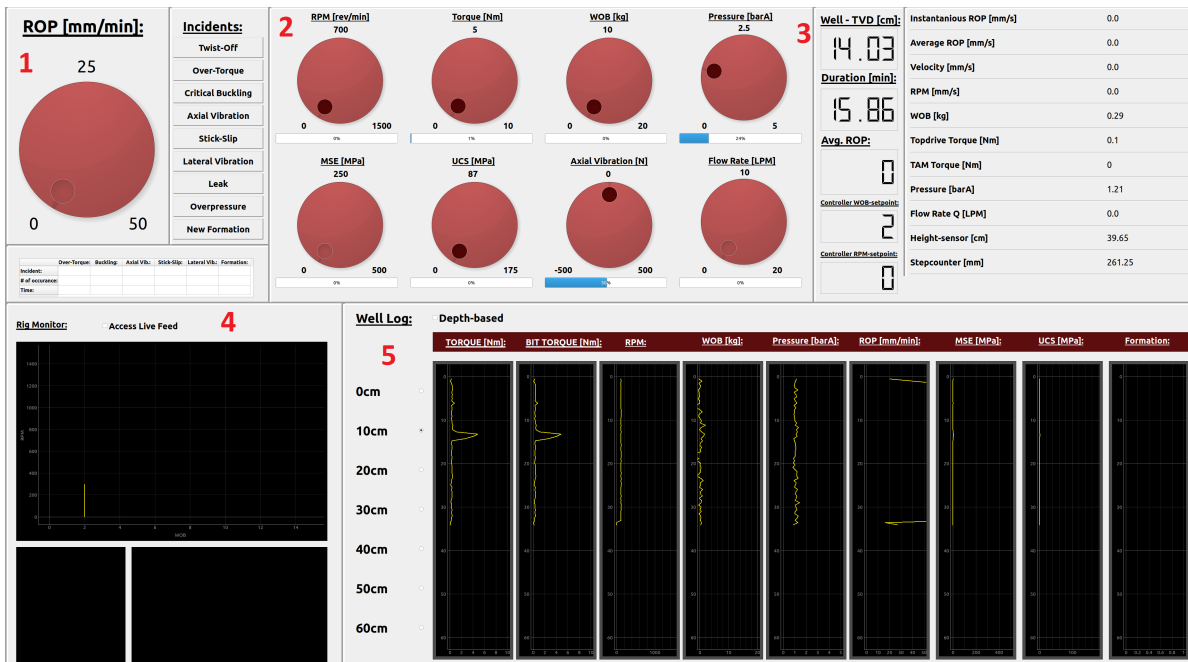
Figure 2.17: HMI design, operation status screen.

1. **ROP (mm/min) and incidents**
   This section shows the current ROP the rig is drilling. Incident marks red if a fault/incident occurred, where the problem handling acts accordingly.

2. **Analog measurements**
   Visualize the current measurement state of the rig.

3. **Digital measurements**
   Show the current depth and digital number measurements.

4. **Rig monitor**
   Live feed from web-cameras on the rig. Currently shows the formation detection search while drilling.

5. **Well log**
   Also saved to the database, and is the real time plot from the measurements/sensor data.

Chapter 3

Theory

Chapter 3 gives the necessary theory behind communication, Kalman filter and EMI/EMC.

3.1 Communication protocols

When operating the top drive at high RPM, vibrations or stuck pipe may lead to equipment being damaged. Therefore the delay must be as small as possible; response time $> 2\ ms$, can cause damage to equipment. Good communication between equipment is therefore important, so that the control system or problem management can make fast decisions, and take rapid caution regarding faults that may occur.

Communication protocols used in the system are SPI; between Arduino and equipment, and CAN; between DAQ - sensors. This setup leads to a small delay, but is still feasible to operate the rig at high RPM, safely.

3.1.1 Serial Peripheral Interface

SPI is a synchronous serial data protocol which micro-controllers use at high speed transmission over short distances, in communication with one or more peripheral devices. [16]
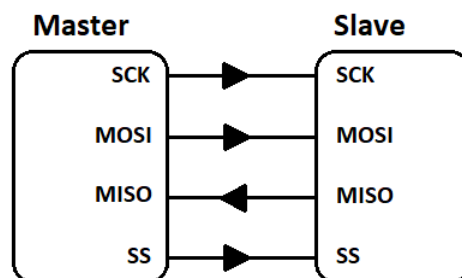
Figure 3.1: SPI setup with one master and one slave. [4]

Between devices SPI uses four physical connections:

- Master In Slave Out (MISO): Slave sending data to master.

- Master Out Slave In (MOSI): Master sending data to slave.

- Serial Clock (SCK): Synchronizes data transmissions to clock pulses by master.

- Slave Select (SS): Master selects a specific device it wants to communicate with by enabling or disable communication.
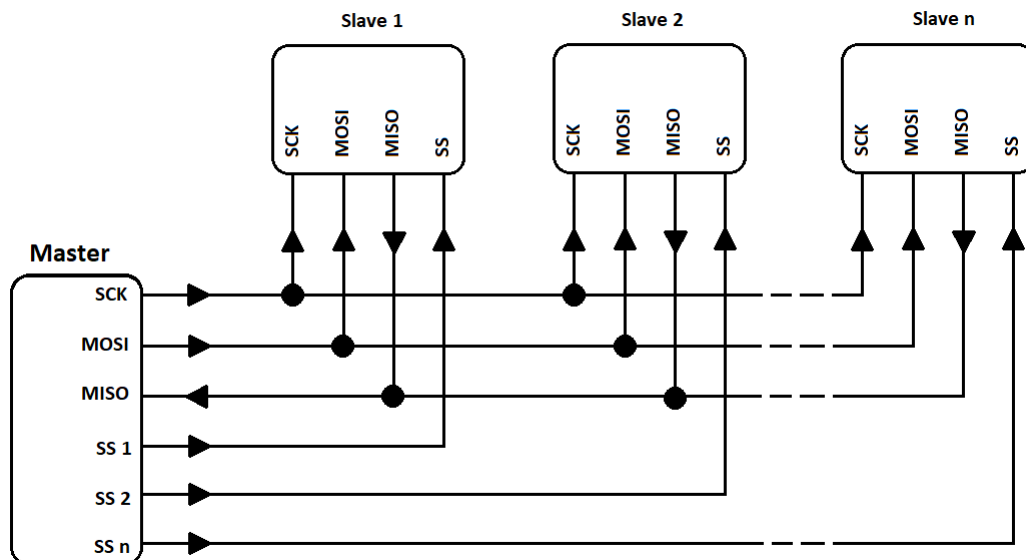
Figure 3.2: SPI setup with one master and multiple slaves. [4]

Multiple slaves can be connected to the master device at the same time. By setting SS state to high, a slave can ignore any messages the master is sending, thus excluding specific devices in the current transmission loop. Setting SS state to low, allows the slave to communicate with the master. On Arduino the limit of SPI devices connected to the micro-controller is simply restricted by the amount of available digital output pins of the Arduino.

3.1.2 Controller Area Network

CAN is a communication protocol commonly used in modern vehicles. Using micro-controllers in network to communicate with each other, and is similar to integrated cable networks. The concept is simple; sensors, computers, etc. are connected on one BUS, which use only one twisted pair in a network cable. Each device connected to the BUS have all electronic information available at all times. Figure 3.3 shows a simple CAN BUS setup. [5]
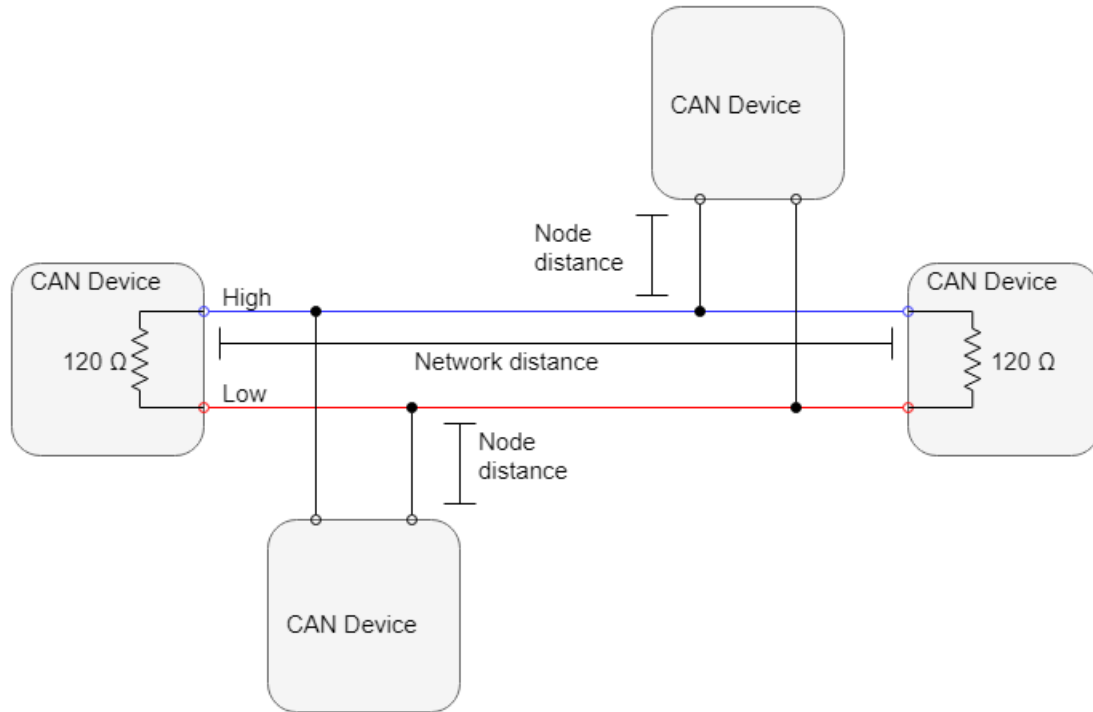
Figure 3.3: Simple CAN description. [5]

On the lab scale drilling rig, CAN is used for communication between sensors and arduinos to DAQ, allowing fast data readings.

3.2 Kalman Filter

The full derivation of Kalman's theory, when deduced in its entirety can be overwhelming. Further derivation of the Kalman's theory is therefore explained in its simplicity, to make it easier to understand. A through derivation of the filter can be studied in the book: Kalman Filtering and Neural Networks.[17] The derivation will include the essential parts of a standard Kalman filter used in this thesis.

Kalman filter is named after Rudolf E. Kálmán, he was collaborating in the development of the filter at the end of 1950's and beginning of 1960's. In the years after up to these days, the filter have had a great impact in the development of newer technologies.

Applications or technology; i.e. navigation and guiding systems in aerospace as well as navigation on the ground (GPS), where the accuracy of position and/or velocity is very crucial. In such applications the Kalman theory improves the estimates of position to vehicles, planes and spaceships. Kalman filter can also be used to collect data from various independent sources to provide an comprehensive estimate compared to estimates created individually.

A Kalman filter is an algorithm that uses numerous measurements over time to produce an estimation of a more accurate measurement. These measurements often contain noise or other uncertainties. By using a recursive method the Kalman filter calculates an optimal estimate of the value. Formally a Kalman filter is the recursive state estimator of an process affected by stochastic disturbances and stochastic noise. [6]

Other implementations of Kalman filter have also been developed, improving the filter to also handle non-linear systems. Some improvements of the original Kalman filter are listed:

- **Extended Kalman filter (EKF);** non-linear version of standard Kalman filter. Considered standard in theory of non-linear state estimation. EKF linearizes estimate of the current mean and covariance.

- **Unscented Kalman filter (UKF);** used in non-linear systems. UKF propagates sampling points through a non-linear map by setting these points around the current state based on its covariance.

- **Ensembled Kalman filter (EnKF);** used in high order non-linear models, where the initial states are highly uncertain, and large number of measurements are available. Often used in wheather forcasting. [18]

3.2.1   Observability

Whether or not the theoretical model of a process is observable, the method gives a solution to the question, by giving the observable states as result. Meaning, the process measurements must depend on the initial conditions one wish to receive information from. Resulting a lower number than the initial states, the process model is not observable.

Given the state-space of discrete time linear system.

$$x(k+1) = \Phi x(k) + \Gamma u(k) \tag{3.1}$$

$$y(k) = Dx(k) + Eu(k) \tag{3.2}$$

Further assume direct link $Eu(k)$ from 3.2 is equal to zero; matrix $E = 0$ or if it cannot be applied, assume vector $u(k) = 0$. The derivations is not time-varying and noise is not applied.

Observability in the *nth-order* plant 3.1 and 3.2 if the matrix

$$O_M = \begin{bmatrix} D \\ D\Phi \\ \vdots \\ D\Phi^{n-1} \end{bmatrix} \tag{3.3}$$

is of rank n, O_M is the *observability matrix.*[19]

3.2.2   Notations

Before the derivation of Kalman filter some notations and words need a brief explanation.

A posteriori: After measurement at time step k. Condition $\hat{x}(k)$ calculated when $u(k)$ and $y(k)$ are known. Previous information is stored in the estimate of condition $\hat{x}(k-1)$.

A priori: Before measurement at time step k. Condition $\bar{x}(k)$ calculated from previous values of $u(k-1)$ and $y(k-1)$, and estimate of previous condition $\bar{x}(k-1)$.

Estimation deviation: Is the difference between true condition $x(k)$ (unknown) and A posteriori estimate, $\hat{x}(k)$. Estimation deviation can be written, $\tilde{x}(k) = x(k) - \hat{x}(k)$.

Table 3.1: Listings of parameters used in the derivations of Kalman filter. It is common to assume $E(k) = 0$ and matrices not time-varying at time step k. [6]

Parameter	Description	Dimensions
$x(k)$ and $x(k+1)$	is the state at time step k and k+1 respectively	n x 1
$u(k)$	control input at time step k	s x 1
$v(k)$	process noise at time step k	n x 1
$y(k)$	actual measurement at time step k	l x 1
$w(k)$	measurement noise at time step k	l x 1
$\Phi(k)$	state transition matrix at time step k	n x n
$\Gamma(k)$	control gain matrix at time step k	n x s
$\Omega(k)$	Disturbance matrix at time step k	n x n
$D(k)$	measurement matrix at time step k	l x n
$E(k)$	direct link matrix at time step k	l x s
Q	auto-covariance matrix for process noise $v(k)$ k	n x n
R	auto-covariance matrix for measurement noise $w(k)$ k	l x l
$K(k))$	optimal kalman gain, sum of diagonal elements in $\hat{P}(k)$	n x l
$\bar{K}(k)$	prvious optimal kalman gain value	n x n
$\hat{P}(k)$	covariance matrix to a posteriori estimation deviation	n x n
$\bar{P}(k)$	covariance matrix to a priori estimation deviation k	n x n

Further the Kalman filter uses the condition vector and various estimates of it

- $x(k)$, true condition vector at time step k. Unknown and true value for the system condition.

- $\hat{x}(k)$, A posteriori condition estimate.

- $\bar{x}(k)$, A priori condition estimate at time step k.

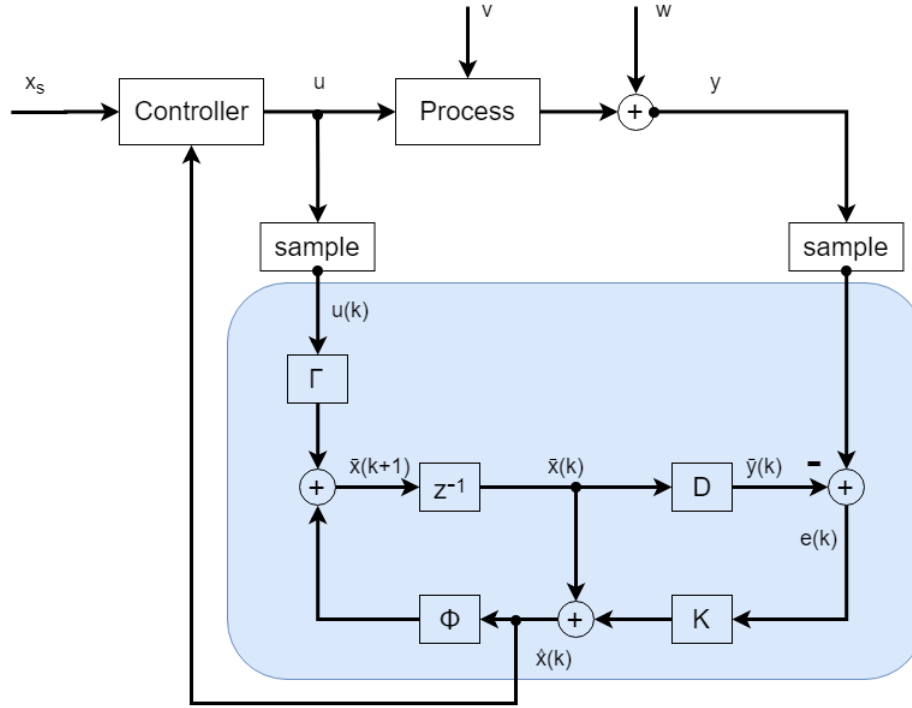- $\tilde{x}(k) = x(k) - \hat{x}(k)$, estimation deviation at time step k.

Figure 3.4: Block diagram of a standard discrete Kalman filter. [6]

x_s is a setpoint. Controller also gets its input from a state estimation $\hat{x}(k)$. Process input u sent from the controller and output the measurement y, both are sampled and sent as inputs to the Kalman-filter. **K**, Kalman gain, is normally calculated for every time step k, but is set as a constant in this figure. Covariance matrices $\bar{P}(k)$ and $\hat{P}(k)$ is used for calculating **K**, where $\hat{P}(k)$ gives a estimate of the uncertainty in the state estimates. For non-linear systems (EKF) the matrices Φ and D will also be time variant, which is then calculated for every time step, as an linearization around the operation point.

Equations (3.4) to (3.8) is the recursive algorithm, with values before time step k and $(k-1)$ known.

$$\bar{x}(k) = \Phi\hat{x}(k-1) + \Gamma u(k-1) \tag{3.4}$$

$$\bar{P}(k) = \Phi\hat{P}(k-1)\Phi^T + Q \tag{3.5}$$

$$K(k) = \bar{P}(k)D^T(D\bar{P}(k)D^T + R)^{-1} \tag{3.6}$$

$$\hat{x}(k) = \bar{x}(k) + K(k)[y(k) - D\bar{x}(k)] \tag{3.7}$$

$$\hat{P}(k) = (I - K(k)D)\bar{P}(k) \tag{3.8}$$

3.3   Electromagnetic Interference

Regarding EMI, the laboratory drilling rig suffered allot from the disturbance. EMC measures was not considered in the 2017 design of the rig, which had an enormous impact in the data quality, thus receiving and handling corrupted sensor data. In the 2018 design, EMC has been improved, and sensitive parts have been isolated, which is one of the biggest improvement in the new design. Regulation and theory of EMI and EMC are explained briefly.

One of the fundamental forces of nature is electromagnetism, which holds matter together. It can be used to describe the magnetic field around an electric wire, by the flow of current. When coiling a wire, electric current increases over a small distance, thus increasing the magnetic field.

Electric motors use the coiling of wire to generate a magnetic field. The magnetic field in the motor then generates a force with a magnet, causing electrical energy. Energy generated from the magnetic field is then converted into physical movement.

Electromagnetic interference (EMI) can be described as the distortion between different magnetic fields; e.g. one generated from a motor and the other following an electrical current in a cable, thus interfering with one another. The amount of EMI is dependant on the current that flows through a cable or coil. A cable transmitting data from a sensor will also generate a magnetic field, but is more sensitive to the disturbance. Corrupted data from EMI is hard and impossible to remove in digital filters, because the filtered data is identical to the real-data. Digital filters remove noise in signal, but removing noise caused by EMI will result in filtering real-data, if the disturbance is to extreme. [20]

In an ideal process the EMI is reduced to not existing, but in the real world that is not the case. Therefore in order to handle EMI, one have to understand how the electrical system and the environment around is operating. Introducing electromagnetic compatibility (EMC), describing how well sources of EMI are handled and reduced; in addition to shielding of sensitive equipment.

Planing distribution systems with EMC measures [21]:

- Distribution facility must be planed carefully.

- Devices transmitting large effects, such as transformers, main distributors, subdivisions, rail and cable routing, shall have sufficient distance (and shielding) to areas containing noise sensitive equipment.

- For precaution, using shielded cables everywhere will always come to the equipment's favour, and it is the grounding of the screen that determines the effect of the display.

- Electrical disturbances can easily propagate between one cable and another if they are placed beside each other in rails or cable routings.

- When planing and installation of distribution systems, technician is always obliged to follow regulations regarding protective earthing.

- EMC earthing is to lead noisy current in the desired path, and away from sensitive equipment or cables.

As mentioned above, projects regarding distributed systems is always obliged to follow current regulations regarding EMC-earthing and the overall installation. Refer to applicable regulations, as of March 2018:

- **EMC directive (European Commission)**, Directive 2004/108/EC relating to electromagnetic compatibility and repealing Directive 89/336/EEC. [22]

- **FEU**, regulation regarding electrical equipment (in norwegian).[23]

- **NEK EN 60 204-1**, Safety of machinery - Electrical equipment of machines - Part 1: General requirements. It is the choice of engineering of electrical equipment and electrical installations on machines.[24]

- **NEK EN 60 439-series**, consist of three parts: [25]

    - Part A, general requirements of electrical low voltage panel design.
    - Part B, electrical low voltage boards for special purposes.
    - Part C, guide, how to specify electrical low voltage panels.

- **NEK 700:2016**, consists of three main parts (701-703) and is the planing of cabling installations in buildings and outdoor. Secures a minimum requirement of quality in every aspects of infrastructure and information-technology. [26]

Chapter 4

Control and modelling

Chapter 4 is the work that this thesis collaborate to the project. Drill string dynamics is developed using physics theory behind a drill pipe. Drill string model is also further used in experiments through a simulation in Simulink. Kalman filter is used to improve sensor measurements. Results considering Kalman filter will be used to analyze the estimated measurements. Kalman filter is therefore not used in the control system this year.

4.1   Control system

The control system uses the similar structure as in 2017, except now using the HBM-DAQ amplifier for sensor readings. It is divided into three separated control loops; Rotation, hoisting and circulation. Each system uses an arduino micro-controller to handle separated closed loops. A proposed improvement for the control structure is presented for this thesis.
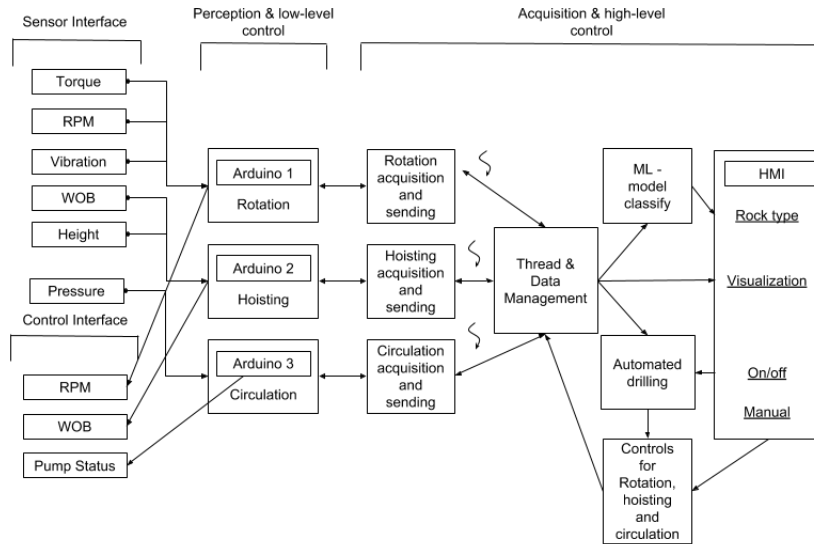
Figure 4.1: Communication architecture.

Sensor interface: Each sensor contributes to the control system by receiving real-time measurements and conditions of the process. Torque, RPM and vibration measurements send raw data to the rotation system. WOB calculation and height measurements send data to the hoisting system. Pressure transmitter sends data to circulation system.

Perception & **low-level control:** This is where the calculations for control are executed. Rotation system uses measurements to calculate the RPM. Hoisting use measurements to calculate WOB. Circulation system outputs the pump status. Low level control also communicates between high-level control to handle raw sensor measurements, by the HBM-DAQ amplifier. A solution to improve the control system in figure 4.2 consists of multiloop PID control, and Kalman filter for PID parameter estimation.

Acquisition & **high-level control:** High-level control handles data received by the low-level control, to monitor the condition of the system. This level controls the process and monitors the conditions to ensure operations running in safe windows.

4.1.1 Proposed control system

A new control system is proposed in this thesis. To control RPM and WOB by introducing multiloop control system. Following this way the two controllers for rotation and hoisting can collaborate in the process to optimize ROP.
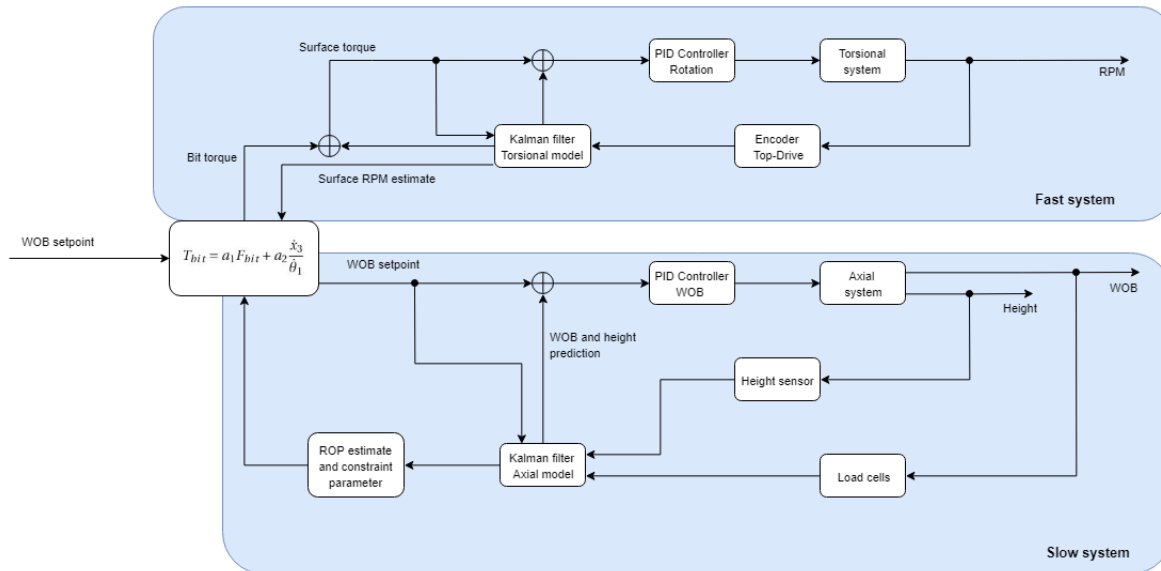
Figure 4.2: Multiloop PID control of RPM and WOB.

Figure 4.2 shows the structure of control system. Block containing equation:
$T_{bit} = a_1 F_{bit} + a_2 \frac{\dot{x}_3}{\theta_1}$, variables given later, is the representation of torque on bit, where a_1 and a_2 are unknown. Rotational system is considered to be the fast system, since it operates at high speeds. Operating at high RPM will also require quick actions from problem handling, to prevent any incidents while drilling. Hoisting system; WOB and height, is generally operating at low speed through the operation. WOB control uses the measurement from height and LC sensors in order to estimate the WOB. In both systems Kalman filter is integrated in order to estimate good measurement estimations from the sensors, thus optimizing the PID parameters.

4.2 Drill string dynamic model

Drilling a hole in a formation; either it is cement, sandstone, granite, etc. the force applied to the drill string will cause vibrations. These vibrations can potentially damage the drill pipe, equipment and the wellbore. In order to understand the vibrations, and the impact, one can associate the model with a mass-spring-damping system, ref. figure 4.3. Spring is the drill pipes degree of materialistic flexibility. Damping is the pressure inside the drill string, higher pressure increases the dampening factor. Drill string dynamics is derived into two separated models; axial and torsional, where both have influence to the process.

4.2.1 Torsional

The torsional model is developed and is similar to the axial model. The two models, torsional and axial have different forces, and elements considered in the applied directions. As for the

physical model, the drill string is considered to be a mass-spring-damping system with three elements, giving three DOF. The model is to estimate the vibrations and movement of the system, for which the controllers are implemented.
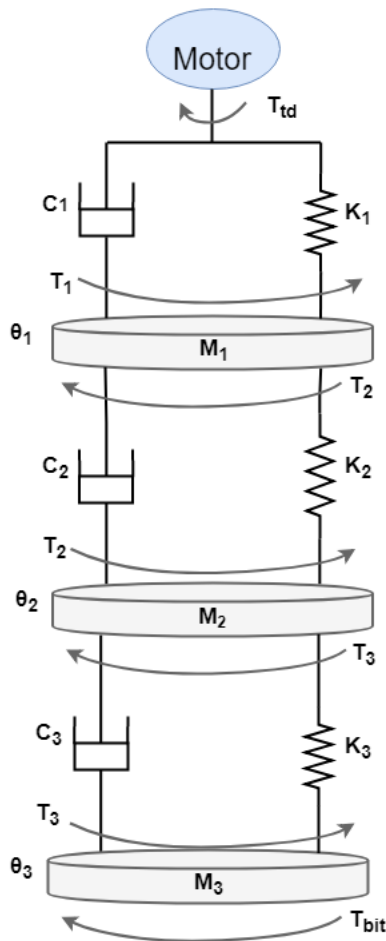

Figure 4.3: Physical dynamic model of an drill string.

T_{td}	top drive torque.
T_{bit}	bit torque.
T_n	torque; drill pipe, BHA and bit.
C_n	damning coefficient.
K_n	spring coefficient.
M_n	mass; drill pipe, BHA and bit.
θ_n	angle; drill pipe, BHA and bit

Torsional is the rotation of the drill sting, and uses the stiffness of the system rather than the masses. The model measures the vibration laterally. [27]

The simplified solution with initial conditions can be expressed:

$$J\ddot{\theta} + C\dot{\theta} + K\theta = T \tag{4.1}$$

When increased to three DOF like figure 4.3, the system can be deduced:

$$[J]\ddot{\theta} + [C]\dot{\theta} + [K]\theta = T \tag{4.2}$$

Where,

$$J = \begin{bmatrix} J_1 & 0 & 0 \\ 0 & J_2 & 0 \\ 0 & 0 & J_3 \end{bmatrix} \tag{4.3a}$$

$$C = \begin{bmatrix} c_1 + c_2 & -c_2 & 0 \\ -c_2 & c_2 + c_3 & -c_3 \\ 0 & -c_3 & c_3 \end{bmatrix} \tag{4.3b}$$

$$K = \begin{bmatrix} k_1 + k_2 & -k_2 & 0 \\ -k_2 & k_2 + k_3 & -k_3 \\ 0 & -k_3 & k_3 \end{bmatrix} \tag{4.3c}$$

$$\theta = \begin{bmatrix} \theta_1 \\ \theta_2 \\ \theta_3 \end{bmatrix} \tag{4.3d}$$

$$T = \begin{bmatrix} 0 \\ 0 \\ -T_{bit} \end{bmatrix} \tag{4.3e}$$

Since the model is in the torsional direction, x (position) from axial model is changed to θ, which is the angle (rad/s) of the drill string. M (mass) is changed to J (joint). Given the drill string model with three DOF, the equations become:

$$
\begin{aligned}
T_1 &= -c_1\dot{\theta}_1 - k_1\theta_1 \\
T_2 &= c_2(\dot{\theta}_1 - \dot{\theta}_2) + k_2(\theta_1 - \theta_2) \\
T_3 &= c_3(\dot{\theta}_2 - \dot{\theta}_3) + k_3(\theta_2 - \theta_3)
\end{aligned}
\tag{4.4}
$$

$$
\begin{aligned}
J_1\ddot{\theta}_1 &= -c_1\dot{\theta}_1 - k_1\theta_1 - c_2(\dot{\theta}_1 - \dot{\theta}_2) - k_2(\theta_1 - \theta_2) \\
J_2\ddot{\theta}_2 &= c_2(\dot{\theta}_1 - \dot{\theta}_2) + k_2(\theta_1 - \theta_2) - c_3(\dot{\theta}_2 - \dot{\theta}_3) - k_3(\theta_2 - \theta_3) \\
J_3\ddot{\theta}_3 &= c_3(\dot{\theta}_2 - \dot{\theta}_3) + k_3(\theta_2 - \theta_3)
\end{aligned}
\tag{4.5}
$$

Where

θ_i angle of joint i

k_i stiffness coefficient for string section i

c_i internal damping coefficient for string section i

T_i torque from string section i to i+1

T_{td} torque from top drive

T_{bit} torque from bit

j_i inertia from string section i

$$\ddot{\theta}_1 = \frac{1}{j_1}(-c_1\dot{\theta}_1 - k_1\theta_1 - c_2(\dot{\theta}_1 - \dot{\theta}_2) - k_2(\theta_1 - \theta_2))$$

$$\ddot{\theta}_2 = \frac{1}{j_2}(c_2(\dot{\theta}_1 - \dot{\theta}_2) + k_2(\theta_1 - \theta_2) - c_3(\dot{\theta}_2 - \dot{\theta}_3) - k_3(\theta_2 - \theta_3)) \quad\quad (4.6)$$

$$\ddot{\theta}_3 = \frac{1}{j_3}(c_3(\dot{\theta}_2 - \dot{\theta}_3) + k_3(\theta_2 - \theta_3))$$

Changes the states to standard notation, and input to eq. 4.6, applies definitions below:

$$
\begin{aligned}
x_1 &= \theta_1 & x_4 &= \dot{x}_1 = \dot{\theta}_1 & \dot{x}_4 &= \ddot{\theta}_1 \\
x_2 &= \theta_2 & x_5 &= \dot{x}_2 = \dot{\theta}_2 & \dot{x}_5 &= \ddot{\theta}_2 \\
x_3 &= \theta_3 & x_6 &= \dot{x}_3 = \dot{\theta}_3 & \dot{x}_6 &= \ddot{\theta}_3
\end{aligned}
\quad\quad (4.7)
$$

$\dot{x}_1$, $\dot{x}_2$, $\dot{x}_3$ are included to the state space model to get a square system matrix. Inserting the definitions to eq. 4.6 gives:

$$\dot{x}_1 = x_4$$

$$\dot{x}_2 = x_5$$

$$\dot{x}_3 = x_6$$

$$\dot{x}_4 = \frac{1}{j_1}(-(k_1 + k_2)x_1 + k_2 x_2 - (c_1 + c_2)x_4 + c_2 x_5) \quad\quad (4.8)$$

$$\dot{x}_5 = \frac{1}{j_2}(k_1 x_1 - (k_2 + k_3)x_2 + k_3 x_3 + c_2 x_4 - (c_2 + c_3)x_5 + c_3 x_6)$$

$$\dot{x}_6 = \frac{1}{j_3}(k_3 x_2 - k_3 x_3 + c_3 x_5 - c_3 x_6)$$

Equations then give the time-invariant model:

$$\dot{x} = \mathbf{Ax} \quad\quad (4.9)$$

$$
\mathbf{A} = \begin{bmatrix}
0 & 0 & 0 & 1 & 0 & 0 \\
0 & 0 & 0 & 0 & 1 & 0 \\
0 & 0 & 0 & 0 & 0 & 1 \\
-\dfrac{(k_1 + k_2)}{j_1} & \dfrac{k_2}{j_1} & 0 & -\dfrac{(c_1 + c_2)}{j_1} & \dfrac{c_2}{j_1} & 0 \\
\dfrac{k_1}{j_2} & -\dfrac{(k_2 + k_3)}{j_2} & \dfrac{k_3}{j_2} & \dfrac{c_2}{j_2} & -\dfrac{(c_2 + c_3)}{j_2} & \dfrac{c_3}{j_2} \\
0 & \dfrac{k_3}{j_3} & -\dfrac{k_3}{j_3} & 0 & \dfrac{c_3}{j_3} & -\dfrac{c_3}{j_3}
\end{bmatrix}
\tag{4.10}
$$

$$
\mathbf{x} = \begin{bmatrix} x_1 \\ x_2 \\ x_3 \\ x_4 \\ x_5 \\ x_6 \end{bmatrix}
\tag{4.11}
$$

Adding force to the model gives the new time-invariant state space model equation:

$$
\dot{x} = \mathbf{A}x + \mathbf{B}u
$$
$$
y = \mathbf{C}x
\tag{4.12}
$$

Further changing the equations; only the last part (bit) equation changes:

$$
T_3 = c_3(\dot{\theta}_2 - \dot{\theta}_3) + k_3(\theta_2 - \theta_3 - T_{bit})
\tag{4.13}
$$

$$
J_3\ddot{\theta}_3 = c_3(\dot{\theta}_2 - \dot{\theta}_3) + k_3(\theta_2 - \theta_3 - T_{bit})
\tag{4.14}
$$

$$
\ddot{\theta}_3 = \frac{1}{j_3}(c_3(\dot{\theta}_2 - \dot{\theta}_3) + k_3(\theta_2 - \theta_3) - T_{bit})
\tag{4.15}
$$

$$
\mathbf{B} = \begin{bmatrix} 0 \\ 0 \\ 0 \\ 0 \\ 0 \\ 1 \end{bmatrix}
\tag{4.16}
$$

$$
\mathbf{u} = \frac{-T_{bit}}{j_3}
\tag{4.17}
$$

$\mathbf{y}$ is the conditions that are measured in the model, giving:

$$
\mathbf{C} = \begin{bmatrix} 0 & 0 & 0 & 1 & 0 & 0 \end{bmatrix}
\tag{4.18}
$$

Where the fourth element is measurable, which corresponds to $\dot{\theta}_1$; RPM of the top drive.

4.2.2 Axial

Axial model is the up/down movement direction of the drill string. This model uses the masses of the drill string, and measures the vibrations vertically, i.e. when pushing down on the rock. This model was carried out by a Phd. student. The final solution can be expressed, and is similar to the torsional solution as

$$M\ddot{x} + C\dot{x} + Kx = F \tag{4.19}$$

4.3 Torsional model simulation

To test and verify the mathematical torsional model of the drill string, it was implemented in Matlab Simulink. The model is configured accordance to the equations (4.8) in chapter 4.2.1. Simulink model also uses available information on the subject, from MathWorks [28].

4.3.1 Simulink model

First part of the model shows inputs and outputs of the torsional model blocks. It is possible to add input to all three systems in order to simulate force on the respective system. In the real process, the force input comes from the top drive motor, rotating the drill string. If the drill string does not touch the bottom formation, there will be no counter force to the rotation direction. Touching the formation will cause the friction, which will counter the force added from the top drive. The force on the third system, bit, is therefore considered as the input, to this model. It will operate as if force on the bit is already known, however the part that we can control is the top drive.
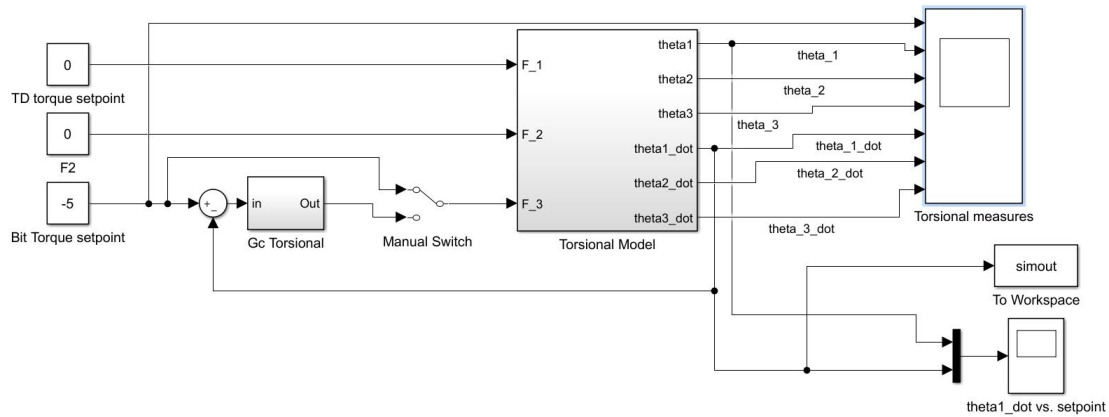
Figure 4.4: System with controller G_c and plant; torsional model. Controlling $\dot{\theta}_1$ and feedback the error. Force on $T_{bit} = -5$.

Figure 4.4 show the force on bit is set to -5 torque (Nm) in accordance to the drill string model in section 4.2.1. Force is given to the bit while top drive torque is controlled. While adding force to the model the initial conditions are set to zero. Setting a force to the measurable initial condition, $\dot{\theta}_4$, gives the response of the system at the given force. A controller is also added to the simulation, which can be turned off, in order to experiment with constant input.
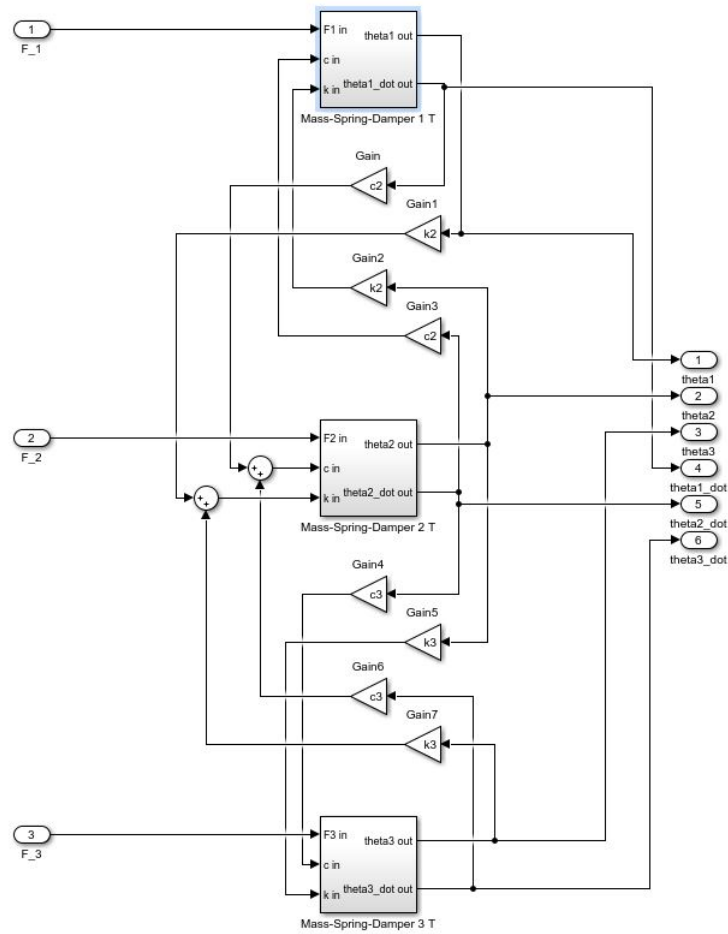
Figure 4.5: Complete mass-spring-damper system.

Figure 4.5 shows the complete torsional model sub-system. Each block consist of one mass-spring-damper system, and is considered one as one DOF. Adding more sub-systems increases the DOF.
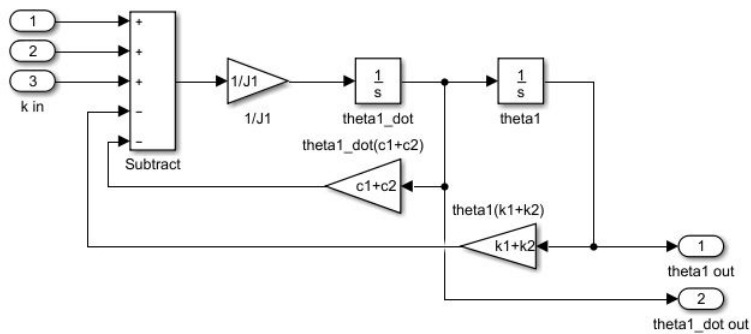

Figure 4.6: Block diagram of the first mass-spring-damper system.

Figure 4.6 represent one mass-spring-damper sub-system. Input to the block is force (initially zero), dampening (c_2) and spring (k_2 from the the second model. The sub-system outputs θ_n position and $\dot{\theta}_n$ velocity.

PID controller block, G_c *torsional*, is shown in figure 4.7. This block is made considering the PID equation (4.20).
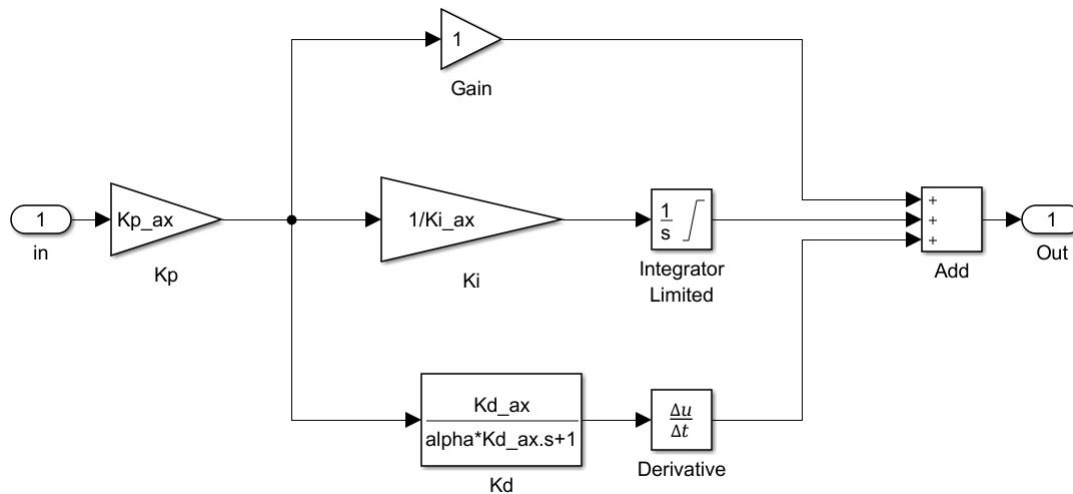

Figure 4.7: PID controller used in the system.

$$u = K_p e + K_i \int_0^t e \, dt + K_d \frac{d}{dt} e \qquad (4.20)$$

Dampening factor of the system is set to $5 * 10^6$ as a standard. Reason for this value is the model stiffness. The true value is not known, and is an assumption, for now. If the factor is higher than $5 * 10^6$ with constant input, the response will dampen as it increases. Setting the dampening factor to zero gives oscillations, which fade-out over time. Figure 4.8 shows the response of the model with the standard dampening.
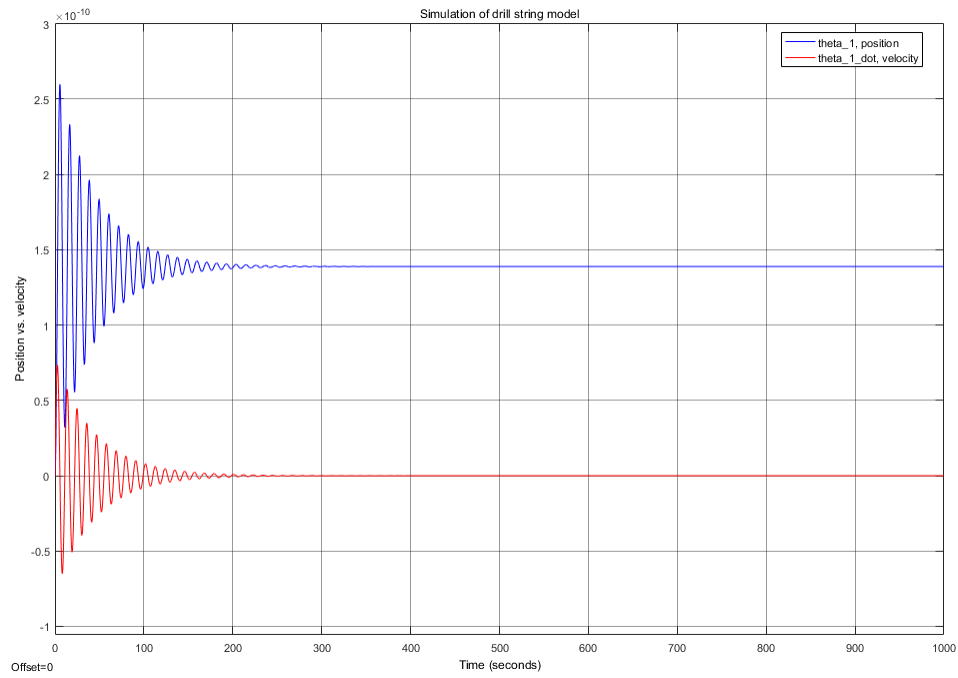
Figure 4.8: Dampening factor $D_r = 5 * 10^6$, standard.

Chapter 5

Experiments and results

Experiments given below are based on simulation results, and are the results of the contributions made through this thesis.

5.1   Simulink simulations

Table 5.1 shows the measurements of the drill string to simulate the torsional drill string dynamics. This gives an estimated response of how a new part or pipe may influence the the process. If logged measurements are given, one can calibrate the dampening factor, and stiffness factor. [Simen Jøsang Nilsen and Ole André Hjelm, master's thesis].

Table 5.1: Drill string measurements used in the simulation experiments.

Measurement	Real measurement value (stiff)
Lengths (L)	
Pipe	914.4 mm
BHA	238.9 mm
Bit	140.0 mm
Outer diameters (OD)	
Pipe	9.525 mm
BHA	27.781 mm
Bit	28.575 mm
Inner diameters (ID)	
Pipe	7.62 mm
BHA	7.62 mm
Bit	7.62 mm
Densities (d)	
Pipe	2700 kg/m^3
BHA	2700 kg/m^3
Bit	7850 kg/m^3
Modulus of rigidity (G)	
Pipe	$69 * 10^9$ Pa
BHA	$210 * 10^9$ Pa
Bit	$164 * 10^9$ Pa
Dampening factor	
D_r	$2 * 10^8$

Measurements from Table 5.1 is further used in calculations 5.1 to 5.4. These calculations estimate the joint, spring and dampening coefficients.

Mass moment of inertia:

$$I_n = (\frac{\pi}{32}) * (OD_n^4 - ID_n^4) \tag{5.1}$$

Spring coefficients:

$$k_n = \frac{G_n * I_n}{L_n} \tag{5.2}$$

Polar moment of inertia:

$$J_n = d_n * I_n * L_n \tag{5.3}$$

Dampening coefficient:

$$c_n = D_r * L_n \tag{5.4}$$

Table 5.2 is the PID parameters used in the simulations. These are found from trial and error, and tuned if measurements of table 5.1 change.

Table 5.2: Control parameters used in the simulations.

PID parameters	
Paramaeter	**Value**
K_p	$36 * 10^9$
K_i	1
K_d	$5 * 10^6$
D_r	$2 * 10^8$

5.1.1 Results from simulation

Simulation is tested through three experiments. Experiments give an indication of how the drill string reacts to different conditions, with drill string measurements.

- Experiment 1: Open-loop system.

- Experiment 2: PID controller added to the simulation.

- Experiment 3: Varying velocity initial condition.

Experiment 1

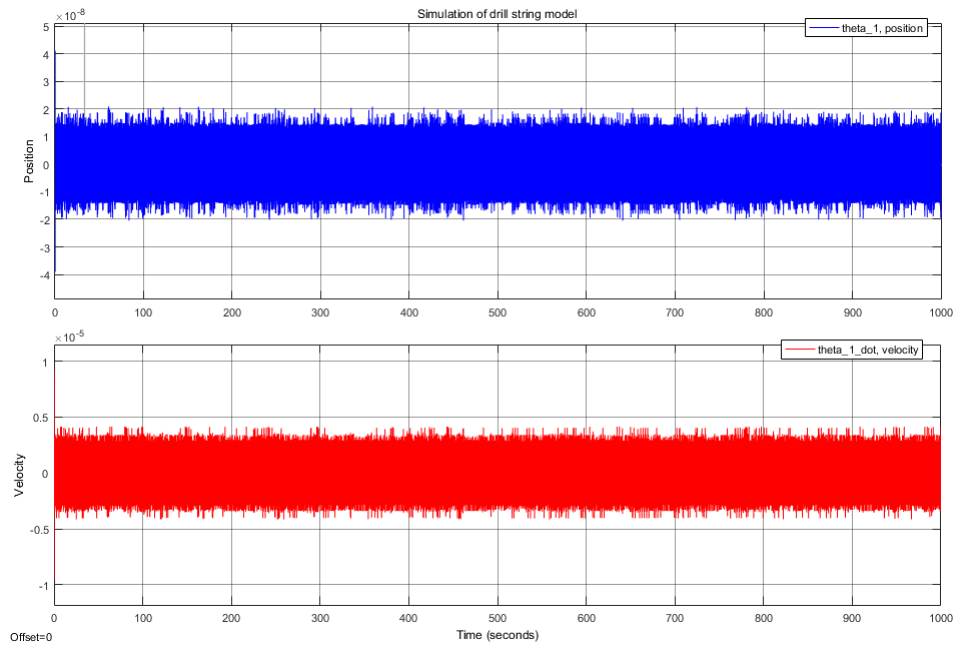First experiment does not have the controller activated, which will give a natural response to a force on the bit.

Figure 5.1: Position versus velocity of top drive, no dampening.

Observed in figure 5.1 with given force (torque) of 5 Nm, the vibrations do not settle and will continue infinitely. Higher dampening settles the vibrations faster, and will not oscillate if dampening is high enough.
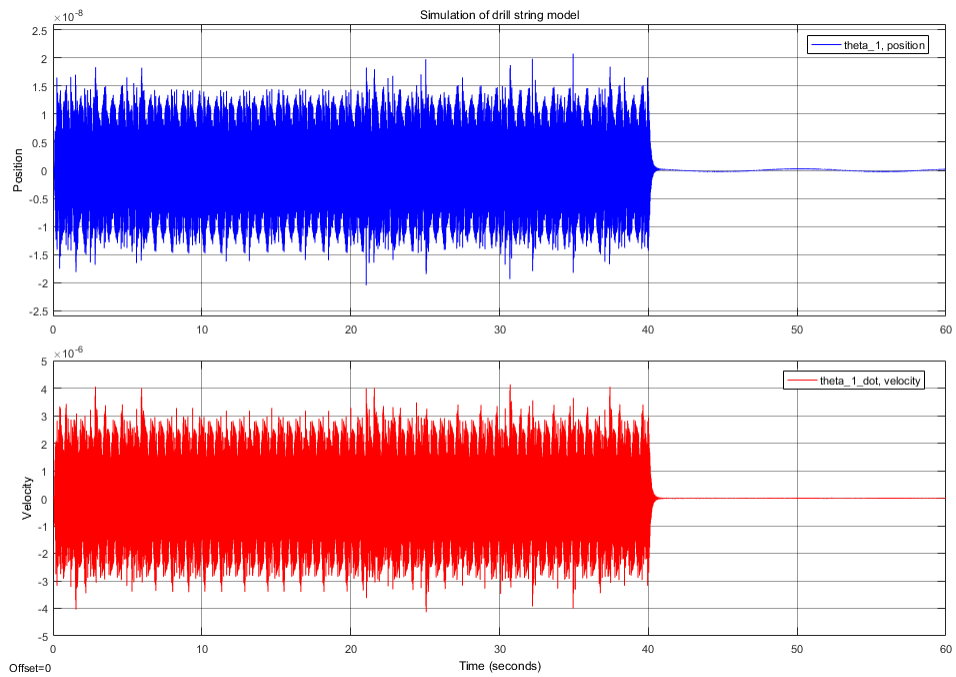

Figure 5.2: Position versus velocity of top drive, with dampening, and step input.

Setting a step input starting at 5 *Nm*, and go to zero after 40 seconds. Figure 5.2 show that the model follows and settling at zero, still with low oscillations. Velocity do not oscillate, when set to zero.
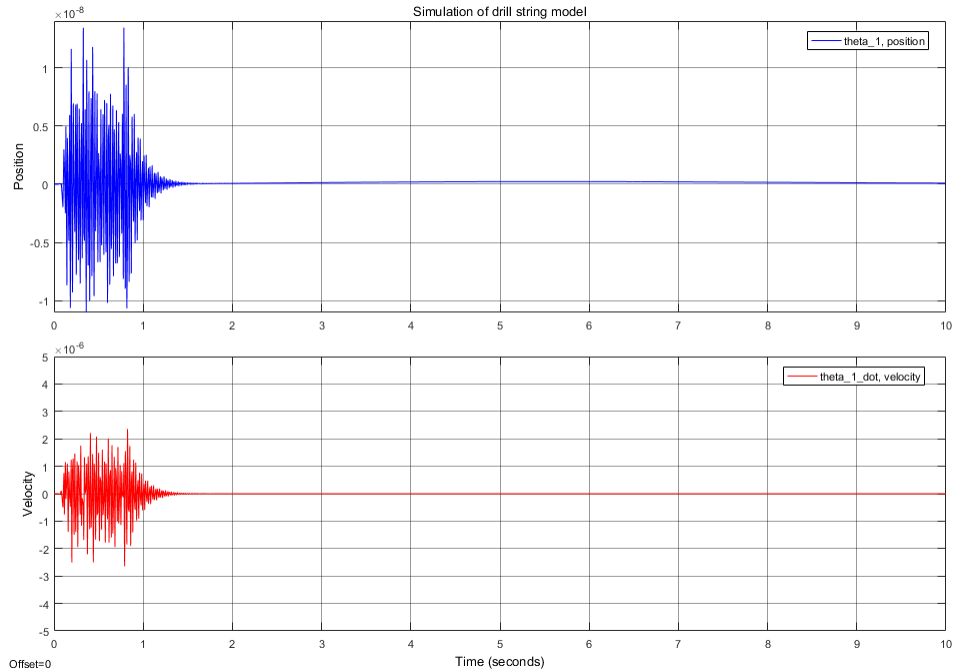

Figure 5.3: Position versus velocity of top drive with dampening.

Figure 5.3 shows the response of the model with dampening. Here the vibrations settles quickly, and have some oscillations the first second.

Experiment 2

In experiment two, the results are critically damped, where the position reaches the setpoint given to the model.
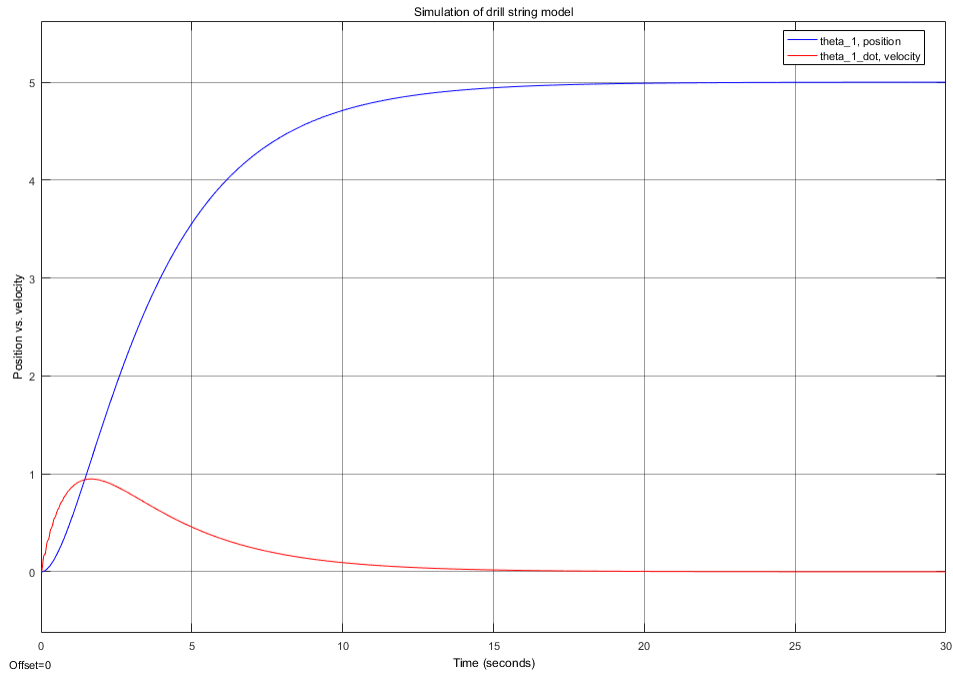
Figure 5.4: Model response with controller on and with dampening.

Figure 5.4 show that position is controlled in this model by adding a force. Position reaches the setpoint, and stay constant even when the velocity reach zero. The position starts to settle at the point where red and blue line meet.
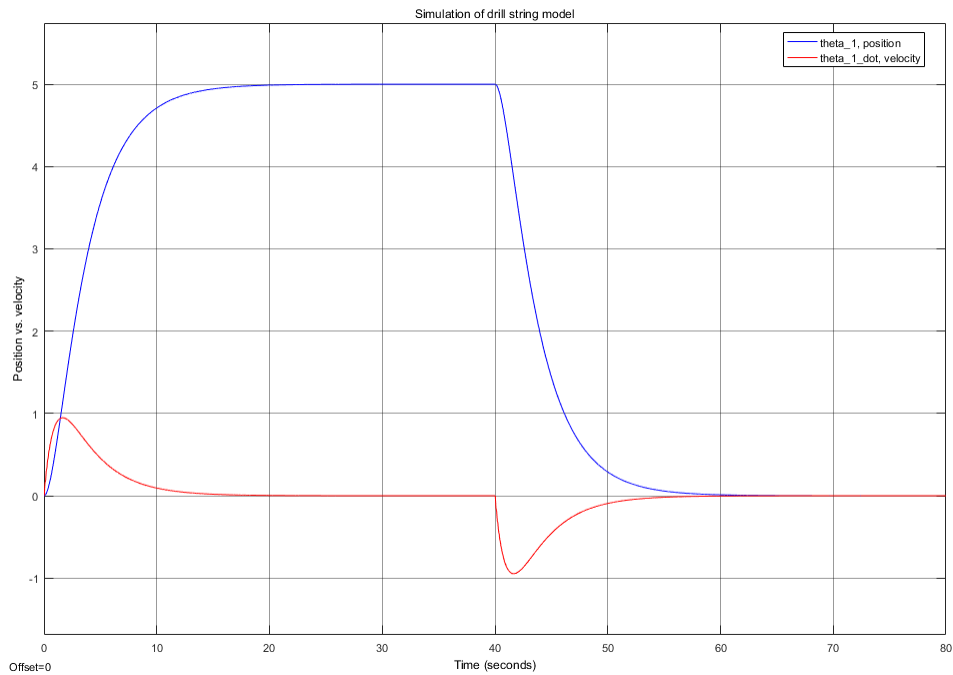

Figure 5.5: Model response with controller on and step input

Adding a step input, shown in figure 5.5, the response reacts to the setpoint at 40 seconds. Letting the force go from 5 Nm to zero show that the velocity goes below zero, forcing the position to zero.

Experiment 3

Experiment three use the initial conditions, where the force input is set to zero. This experiment show how the model reacts at the point of the initial force and going to zero.

Equation (5.5) shows the initial condition $\dot{\theta}_1 = 5$

$$
\begin{bmatrix} \theta_1 \\ \dot{\theta}_1 \\ \theta_2 \\ \dot{\theta}_2 \\ \theta_3 \\ \dot{\theta}_3 \end{bmatrix} = \begin{bmatrix} 0 \\ 5 \\ 0 \\ 0 \\ 0 \\ 0 \end{bmatrix}
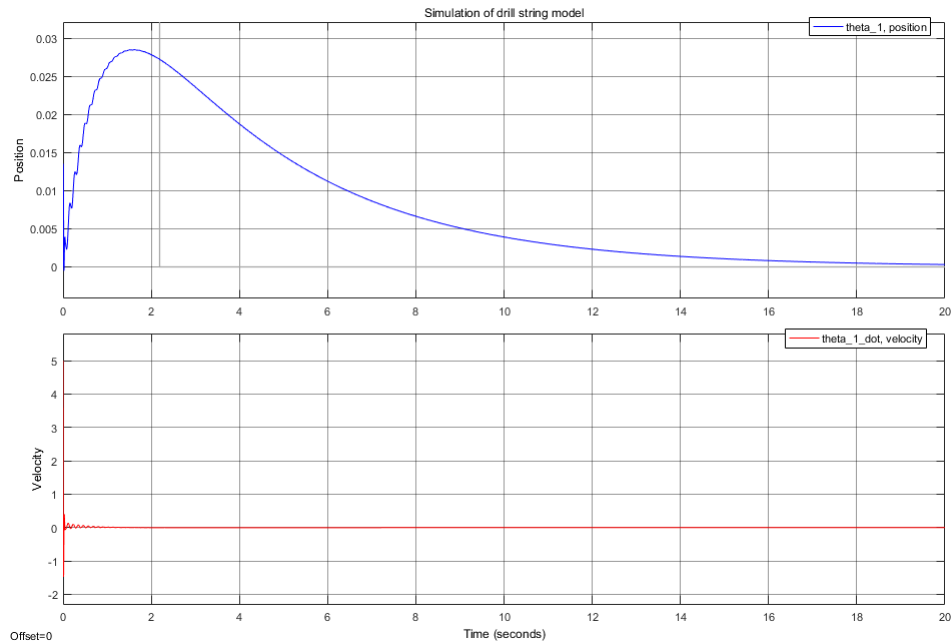\tag{5.5}
$$

Figure 5.6: Top drive response. Initial condition, $\dot{\theta}_1 = 5$
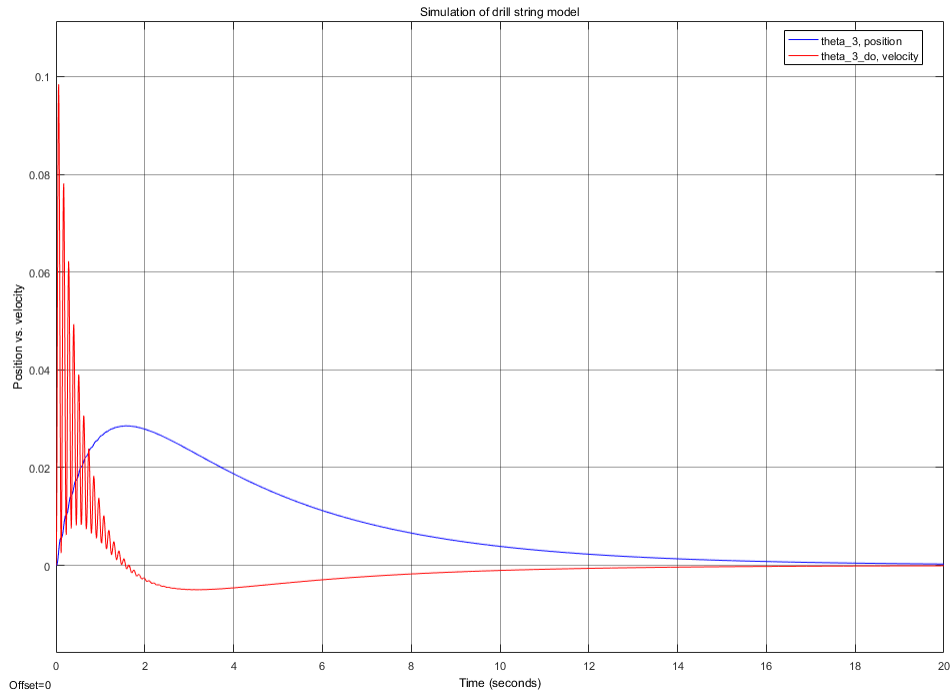
Figure 5.7: Bit response. Initial condition, $\dot{\theta}_1 = 5$

Figure 5.6 and 5.7 is the response of top drive and bit, with initial condition $\dot{\theta}_1 = 5$. θ_1 show a huge displacement response, as the velocity settles quickly. Bit displacement gives the same amplitude as displacement, as should be expected. The bit velocity have smaller amplitudes, though lower velocity than the top drive, due to dampening.

Giving initial condition to $\dot{\theta}_3 = 5$, gives the equation (5.6)

$$\begin{bmatrix} \theta_1 \\ \dot{\theta}_1 \\ \theta_2 \\ \dot{\theta}_2 \\ \theta_3 \\ \dot{\theta}_3 \end{bmatrix} = \begin{bmatrix} 0 \\ 0 \\ 0 \\ 0 \\ 0 \\ 5 \end{bmatrix} \tag{5.6}$$
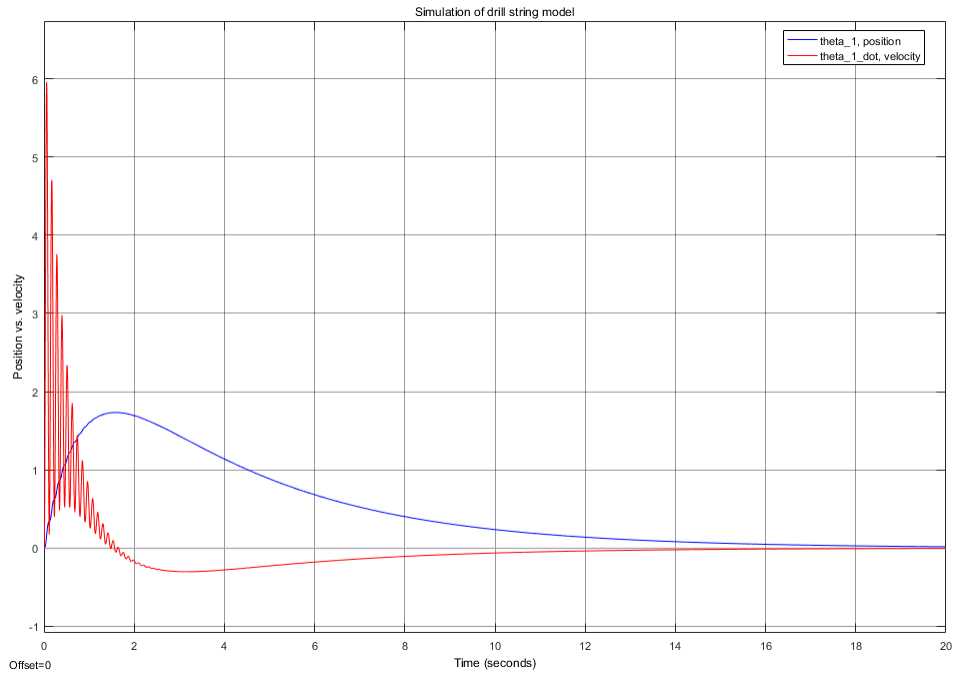
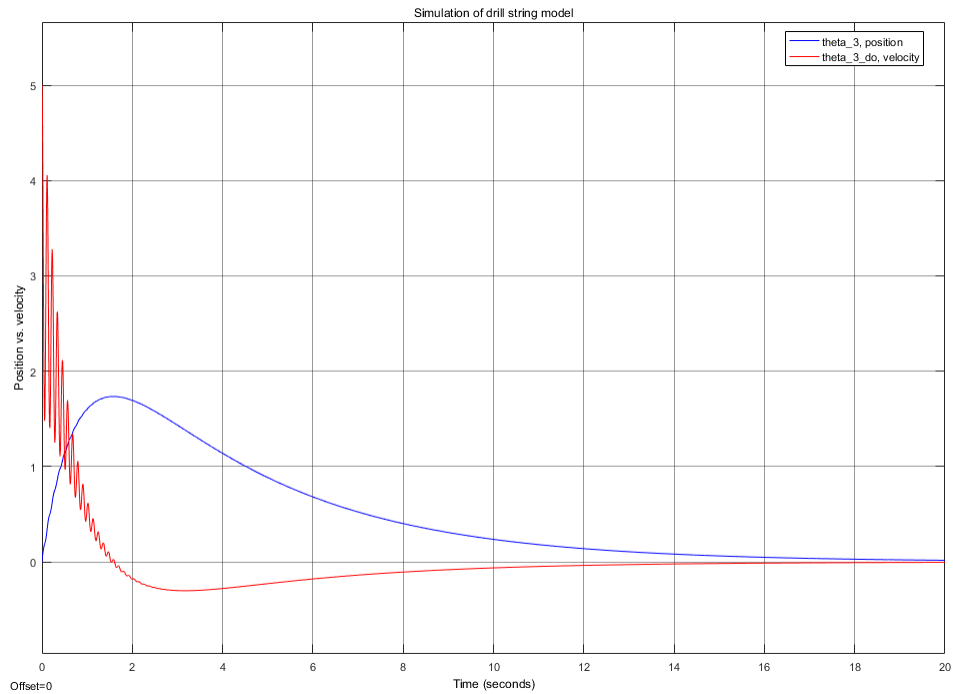**Figure 5.8:** Top drive response. Initial condition, $\dot{\theta}_3 = 5$

Figure 5.9: Bit response. Initial condition, $\dot{\theta}_3 = 5$

Adding initial condition to the bit, $\dot{\theta}_3$, as from the mathematical model, shown in figure 5.8 and 5.9. The velocity is higher on the top drive, and bit velocity dampens faster.
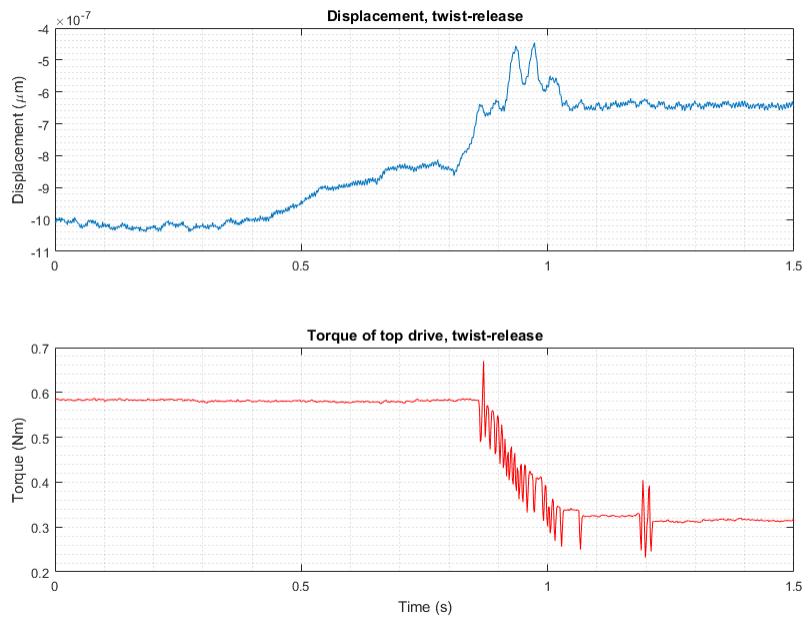
Figure 5.10: Twist-release of drill pipe.

Figure 5.10 shows data from the drilling rig and is the response of a twist-release experiment. This test is carried out by twisting the drill pipe slightly, and release the twist force. This gives gives the response of an initial condition. The figure show that, at the release time, have slightly the same response as shown in the simulation.

5.2 Electromagnetic Interference

Before any testing could be executed, the rig needed shielding and relocation; cables and arduinos, due to high amount of EMI and vibrations. This part is done in order to compare the result of the actions taken in order to reduce EMI.
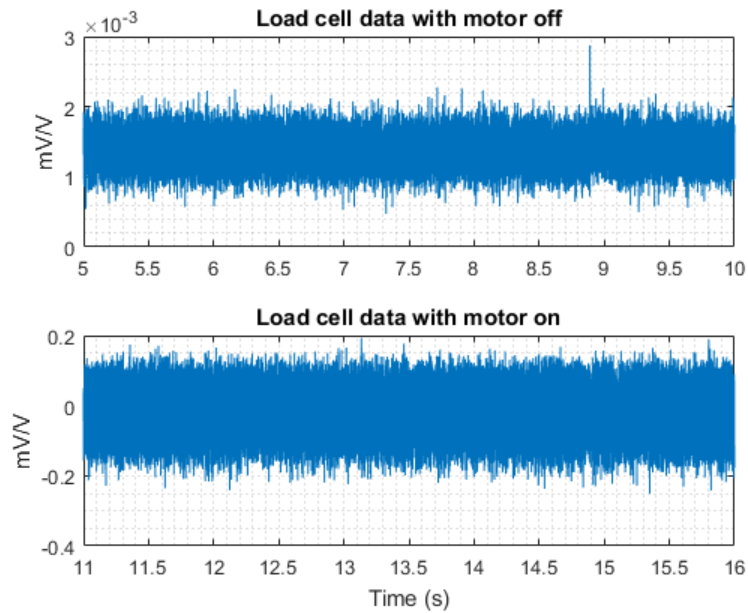
Figure 5.11: Old load cell measurements using HBM DAQ amplifier at 9600 Hz.

Load cell data from figure 5.11 show that the amplitudes are higher when the motor is on. Amplitude will further increase as the motor RPM increases.

Figure 5.12: Old FFT of load cell measurements

Figure 5.12 show more information about the measurement. The load cell measurement is transferred to the frequency domain with FFT (fast fourier transform). As the motor is off, there

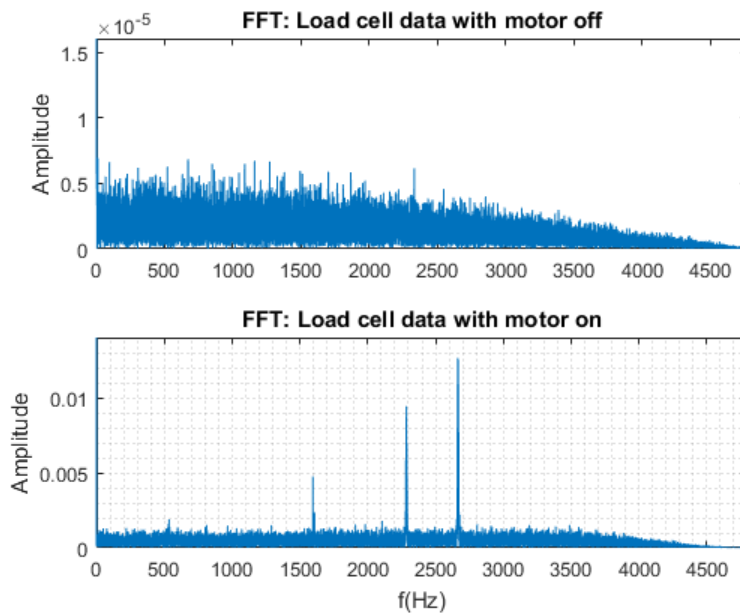are still noise, this comes from environmental conditions, and might not always be the same. Turning on the motor increase the noise in the signal, corrupting it as the speed increases. Response also show highest peaks at high frequencies; 1596 Hz, 2285 Hz and 2667 Hz.
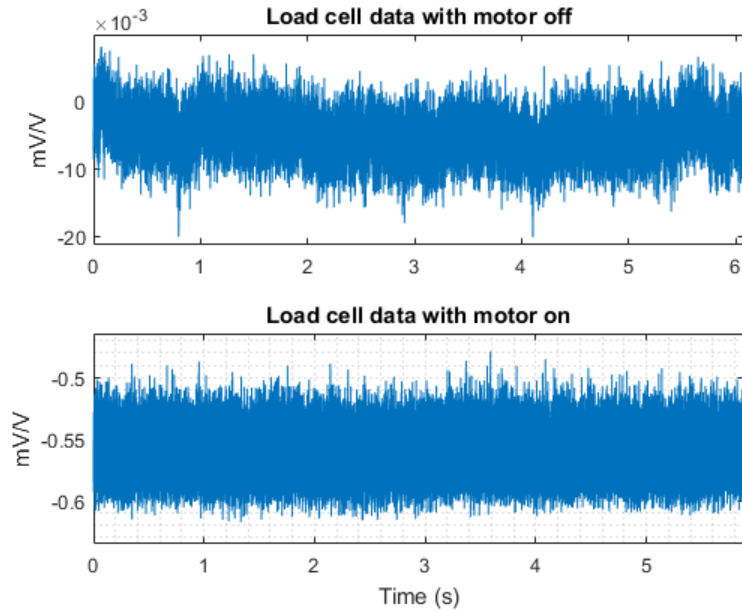

Figure 5.13: New load cell measurements using HBM DAQ amplifier at 9600 Hz.

Shielding cables have reduced the environmental noise slightly, and the noise exposure from the motor have also been reduced, shown in figure 5.13.
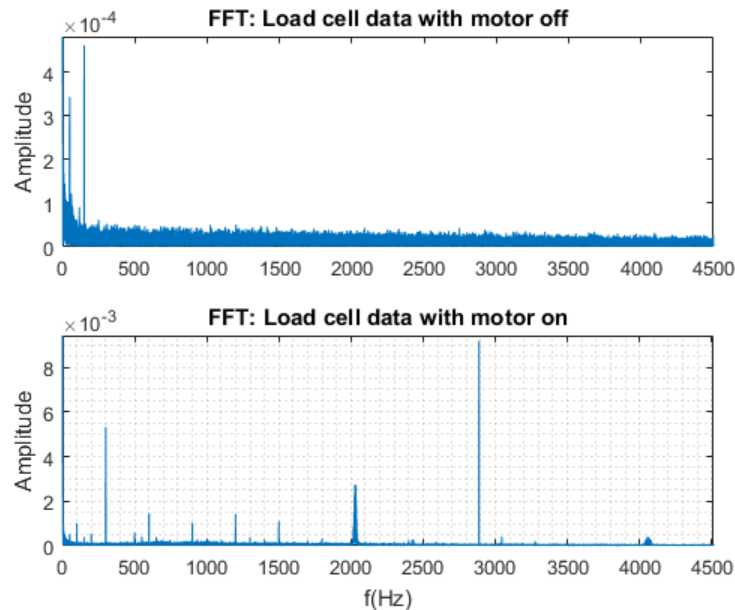
Figure 5.14: New FFT of load cell measurements.

FFT of the measurement show that the environmental noise is still a issue. But do not corrupt the data in the matter that it causes problems in operation. Motor on reveal more peaks at lower frequencies now, than before. The overall noise have been reduced.
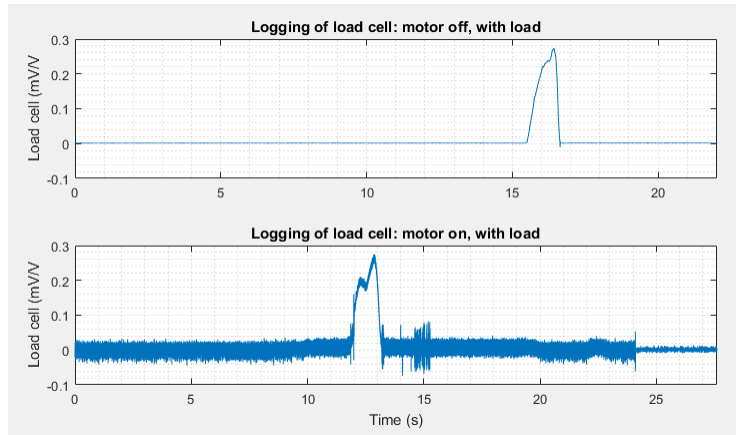
Figure 5.15: Old load cell measurements with load.

Figure 5.16: New load cell measurements with load.

Comparing figure 5.15 and 5.16, the new system have less noise in the data when the motor is on. This gives more accurate WOB calculation, and better control of the drilling rig.

5.3 Kalman filter

This section gives the result analysis of the Kalman filter. The Kalman filter used on the measurement data set do not use the state space model of the process. Program reads sensor data, estimates the a posteriori estimate of the measurement. Auto-covariance matrix Q, process noise, is manually tuned in order to fit the data.
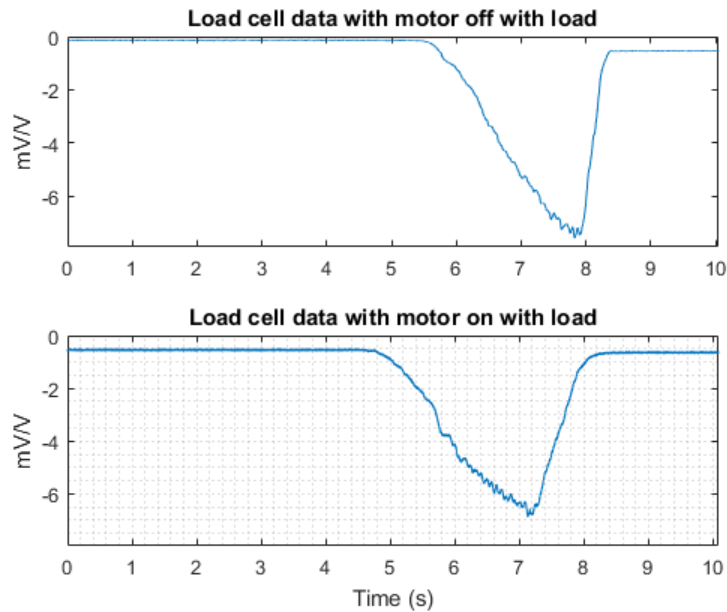
Kalman filter is tested in order to analyze if it is useful for future implementation on the drilling. Implementing the filter means to reduce the time delay and increase WOB accuracy. Data set tested in this thesis is therefore from the WOB data, which is the output from axial direction modelling of the drilling rig.

Considering equations (3.4) to (3.8), WOB is assumed to be constant, and $\Phi = 1$.
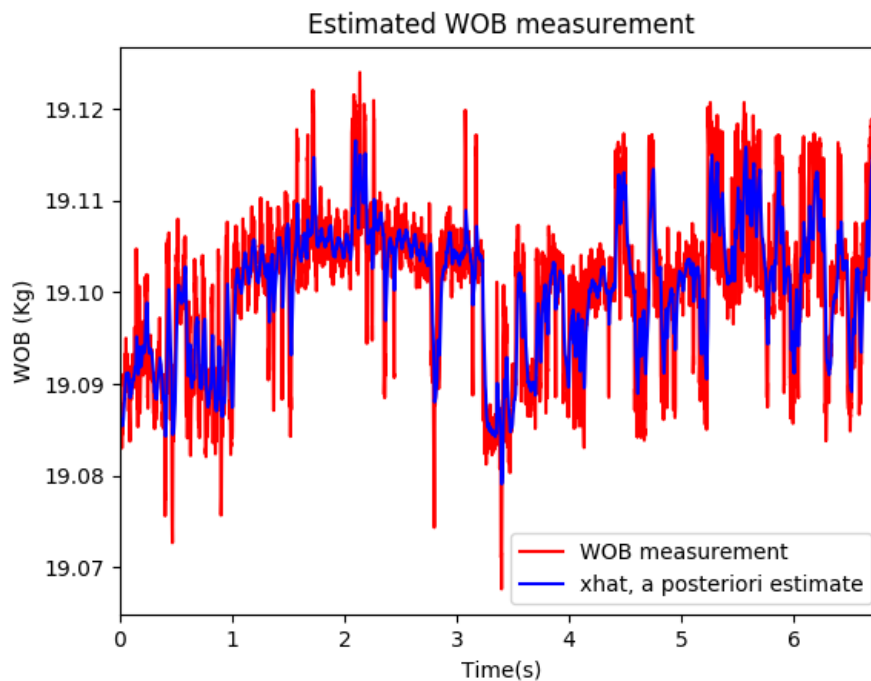
Figure 5.17: Estimated WOB.

Figure 5.17 is from WOB data set, this shows that Kalman filter can increase the accuracy of the data. Better accuracy also gives the PID controller more precise data in order to control the drilling rig. All the oscillations in the data is caused by vibrations in the process, which the Kalman filter reduce, in order to give a precise state.
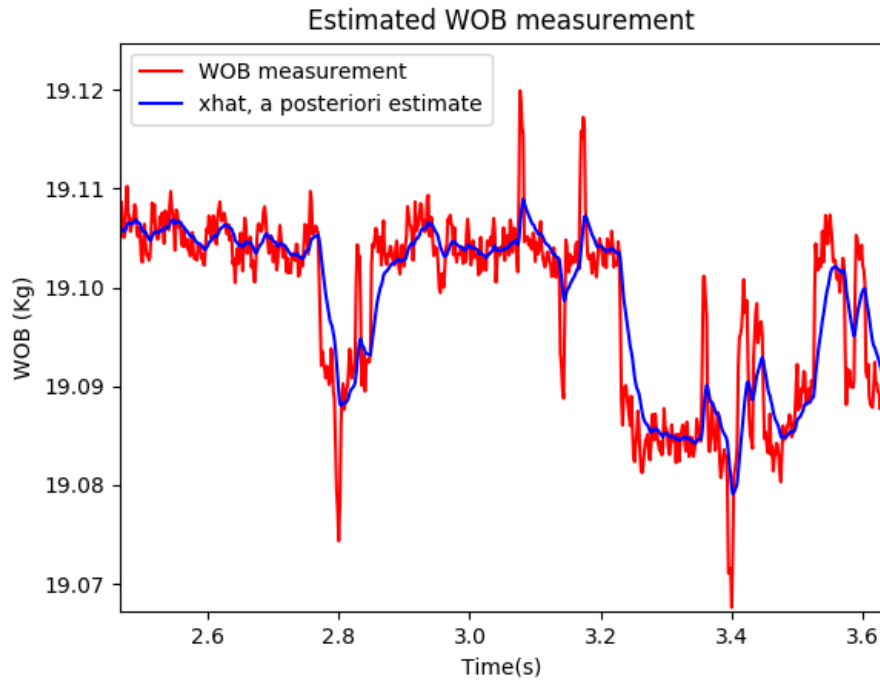
Figure 5.18: Estimated WOB, time 2.6 - 3.6.

Figure 5.18 is zoomed into the figure 5.17, the cropping shows that there are a time shift in the estimated measurement.

Chapter 6

Conclusion

In this thesis, drill string modelling for torsional direction have been deduced and simulated. Control system part became theoretical, where a proposed improvement to it was introduced. Data quality was improved by introducing EMC to the system, which was one of the biggest upgrades on the rig this year. Analysis of the sensor data show that Kalman filter in future implementation, have the possibility to improve the WOB data readings containing vibrations.

Drill string model was designed in order to understand the system conditions. The model is also tested in simulation, which was made in Matlab Simulink. Both the mathematical model and simulation are designed using general rules in physics as well as research papers regarding mass-spring-damper systems. Test results show that the simulation is not perfect. Accurate drill string measurements and more advanced simulation will give better results. With advanced simulation means; introducing friction, motor model, axial model and interruptions one might encounter during drilling. When all these measures are accounted for, one can start to simulate the process, and should be very close to results received on the drilling rig. Simulation results of the torsional model show that it is promising. When compared to real torque data, and given initial condition to the simulation, the results show close relations to one another.

Control system in this thesis gives an idea of how the hoisting and rotation system can be integrated to cooperate in the process. Using multiloop control where the slow system handles the control of the less crucial part of the process, for a more accurate control. However in order to implement multiloop control it is recommended to upgrade the micro-controller to a more advanced or use industrial PLC. Arduino is good for simple projects or operations, but as the project advances the micro-controller is to simple. Meaning it cannot handle multiloops or multiple operations, i.e. why there are three arduinos installed on the drilling rig.

Data quality was improved by making the drilling rig EMC; shielding cables, shielded fuse box, move fuse box away from the source. The actions taken improved the data quality for the LC

sensors, which now gives better readings due to less noise. The LC sensors was not moved, and are still affected by the TD motor. However by placing the amplifiers and arduinos away from the motor, still gave better data quality, when comparing old data with new.

Kalman filter was implemented to WOB measurement in order to analyze effects such filter could give. The results show that, implementing Kalman filter to the operation will give better readings of WOB data. Improving the WOB data, can also increase the ROP since the controller will stay more stable than varying. If Kalman filter is to be implemented in according to figure 4.2, the micro-controller must be upgraded. In order to handle multiple loops and advanced calculations.

Recommendation for future work includes multiloop controllers, micro-controller/PLC and advanced simulation. From an advanced model/simulation of the process it is possible to develop a digital twin of the drilling rig. A digital twin is a simulator which have the same response as the real drilling rig. Where the simulation receives commands as the physical rig would get, and handles faults and conditions the same way. National Oilwell Varco (NOV) have developed a digital twin of one of their drilling ships, this simulator is used to train future offshore drillers. To achieve this goal, more research and further development of the process model needs to be prioritized. [29]

Bibliography

[1] Arduino. Arduino due documentation, 23.03.2018. URL `https://store.arduino.cc/arduino-due`.

[2] Forsentek. Documentation: 3 axis load cell 10n 20n 30n 50n 100n 3-axis force sensor, 10.06.2018. URL `http://m.forsensor.com/sale-9906279d-3-axis-load-cell-10n-20n-30n-50n-100n-3-axis-force-sensor.html`.

[3] Zlatko Briševac; Petar Hrženjak; Renato Buljan. Models for estimating uniaxial compressive strength and elastic modulus, 10.02.2016, GRAĐEVINAR 68 (2016) 1, 19-28.

[4] Sparkfun. Serial peripheral interface (spi), retrieved 05.05.2018. URL `https://learn.sparkfun.com/tutorials/serial-peripheral-interface-spi`.

[5] Quatro Knows. Controller area network (can), retrieved 05.05.2018. URL `https://www.quartoknows.com/blog/quartodrives/2016/04/06/controller-area-network-can/`.

[6] Karl Skretting. notat 3, system identification, ele620, 2017. URL `http://www.ux.uis.no/~karlsk/ELE620/notat3.pdf`.

[7] Haakon Hagen; Andreas Jakobsen; Magomed Khadisov. Laboratory drilling rig construction and testing for optimization and problem management. Technical report, University of Stavanger, 2018.

[8] Society of Petroleum Engineers Drilling Systems Automation Technical Section. Drillbotics guidelines international university competition 2017 - 2018. Technical report, SPE, 7 Nov. 2017.

[9] HBM. Quantumx mx840b and mx440b: 24-bit universal measuring amplifier for all common sensor technologies, 25.03.2018. URL `https://www.hbm.com/en/2129/quantumx-mx840b-8-channel-universal-amplifier/`.

[10] Team University of Stavanger. Drillbotics 2018: Rig design principles and phase 1 report. Technical report, Univerity of Stavanger, 2017.

[11] Alexander Trulsen; Erik Andreas Løken. Construction, design and optimization of an autonomous laboratory-scale drilling rig. Technical report, University of Stavanger, 2017.

[12] Schlumberger. Rop definition, 22.03.2018. URL `http://www-cs-faculty.stanford.edu/~{}uno/abcde.html`.

[13] Todd Robert Hamrick. Optimization of operating parameters for minimum mechanical specific energy in drilling. Technical report, West Virginia University, 2011.

[14] Eric Cayeux et al. Automation of lab-scale drilling rig vs full scale rig. Technical report, Society of petroleum engineers, 2017. URL `https://www.onepetro.org/conference-paper/SPE-185898-MS`.

[15] Schlumberger. Ucs definition, 03.05.2018. URL `http://www.glossary.oilfield.slb.com/Terms/u/uniaxial_compressive_strength.aspx`.

[16] Arduino. Spi library, retrieved 05.05.2018. URL `https://www.arduino.cc/en/Reference/SPI`.

[17] Simon Haykin. *Kalman Filtering and Neural Networks*. John Wiley & Sons, Inc., Communication Research Laboratory of McMaster University in Hamilton, Ontario, Canada, 2004. ISBN 9780471464211.

[18] S. Gillijns; O.B. Mendoza; J. Chandrasekar. What is the ensemble kalman filter and how well does it work? *2006 American Control Conference*, July 2006. doi: 10.1109/ACC.2006.1657419.

[19] Norman S. Nise. *Control Systems Engineering*. John Wiley & Sons, Inc., California State Polytechnic University, Pomona, 6th edition, 2011. ISBN 978-0-470-64612-0.

[20] electronics notes. Emi electromagnetic interference basics, 14.06.2018. URL `https://www.electronics-notes.com/articles/analogue_circuits/emc-emi-electromagnetic-interference-compatibility/what-is-emi-basics-tutorial.php`.

[21] Rune Øverland. Emc – elektromagnetisk forenlighet. Technical report, Trainor Automation AS, 2014. URL `https://nfogm.no/wp-content/uploads/2014/02/NFOGM-EMC-artikkel-nr-2.pdf`.

[22] European Commission. Electromagnetic compatibility (emc), directive 2004/108/ec, 2014. URL `http://ec.europa.eu/growth/single-market/european-standards/harmonised-standards/electromagnetic-compatibility_en`.

[23] Nelfo. Forskrift om electronisk utstyr (norwegian), 30.03.2018. URL `https://nelfo.no/Temaer/Elsikkerhet/Lover-forskrifter-og-normer/ Lover-forskrifter-og-normer2/FEU/`.

[24] NEK. Safety of machinery - electrical equipment of machines - part 1: General requirements., 2006. URL `https://www.nek.no/produkter/nek-en-60204-1/`.

[25] Standard Norge. Nek 439 lavspenningstavler og kanalskinnesystem (norwegian), 20.01.2017. URL `http://www.standard.no/fagomrader/elektrofag/elektro/ nek-439_2013/`.

[26] Nelfo. Nek 700 - kablingssystemer (norwegian), 2016. URL `https://nelfo.no/Temaer/IKT1/Lover-og-forskrifter/ NEK-700---kablingssystemer-og-kabel-TV-anlegg/`.

[27] Parimal Patil; Catalin Teodoriu. Model development of torsional drillstring and investigating parametrically the stick-slips influencing factors. *Journal of Energy Resources Technology*, March 2013. doi: 10.1115/1.4007915.

[28] MathWorks. Documentation: Mass-spring-damper in simulink and simscape, 31.05.2018. URL `https://se.mathworks.com/help/physmod/simscape/examples/ mass-spring-damper-in-simulink-and-simscape.html`.

[29] National Oilwell Varco. Advanced simulation technology, 11.06.2018. URL `http:// training.nov.com/whynov/advancedsimulation`.

Appendix A

Codes

A.1   Simple Kalman filter

This code reads a Matlab file, reads a variable from workspace and process the data. Scipy and Numpy libraries must be installed. Pylab is a standard Python library to plot the data.

```python
import scipy.io as sio
import numpy as np
import pylab

class KalmanFilter(object):

    def __init__(self, Q, R):
        self.Q = Q   # Auto-covariance for process noise
        self.R = R   # Auto-covariance for measurement noise
        self.xhat = 0.0   # A posteriori condition estimate
        self.Phat = 1.0   # A posteriori estimation deviation

    def input_latest_WOB_data(self, measurement):
# Predict
        xbar = self.xhat   # A priori condition estimate
        Pbar = self.Phat + self.Q   # A priori estimation deviation
# Update
        K = Pbar / (Pbar + self.R)   # Kalman gain
        self.xhat = xbar + K * (measurement - xbar) # A posteriori condition estimate
        self.Phat = (1 - K) * Pbar   # A posteriori estimation deviation

    def get_latest_estimated_measurement(self):
        return self.xhat

if __name__ == "__main__":
```

```python
26    # Get data from .MAT (matlab file) or data matrix
27        data_read = sio.loadmat(r'D:\motor_off_600Hz.MAT', struct_as_record=False)
28    # Relevant data from matlab file
29        WOB_data = data_read['Channel_5_Data']
30    # Sampling time of the data set
31        SamplingTime = data_read['Channel_1_Data']
32    # Length of data set.
33        iteration_count = len(SamplingTime)
34    # xrange for Python 3.6 and range for 2.7 (both 32 bit)
35        xrange=range
36
37    # Standard deviation of measurement data set
38        measurement_std = np.std([WOB_data * 2.0 - 1.0 for j in xrange(iteration_count)])
39
40    # Defining noise measurement
41        Q = 0.0009e-6
42        R = measurement_std ** 4
43        kalman_filter = KalmanFilter(Q, R)
44        xhat_est = []
45
46    # Get the latest measurement
47        for iteration in xrange(0, iteration_count):
48            kalman_filter.input_latest_WOB_data(WOB_data[iteration])
49            xhat_est.append(kalman_filter.get_latest_estimated_measurement())
```

A.2 Matlab

Attached Matlab scrip, function and data files in this thesis:

- **Freq_analysis**: Function to calculate the FFT of data set.

- **kalman_func**: Kalman filter function.

- **sim_3DOF_mass_spring_damping_torsional**: Simulation of the torsional drill string model.

- **dataset_plotting_torsional**: Plotting of data and reading data set. Uses *Freq_analysis* to transform data set from time domain to frequency domain.

- **SIMULINK_parameters**: Drill string, PID and Initial condition parameters used in *sim_3DOF_mass_spring_damping_torsional*.

- **motor_off_600Hz**

- **motor_off_9600Hz**

- **motor_on_9600Hz**

Appendix B

Equipment manuals

Manuals is found in attachments followed by this thesis report.

B.1   Sensors

B.2   Pump and Motors

B.3   Micro-controller and QuantumX DAQ

B.4   Schematics